

**Electron microscopic studies on accessory minerals  
from Cape Ashizuri Ring Complex, Kochi, SW Japan:  
With special reference to unusual internal textures of  
zircon and the trace element chemistry**

Hiroki Hayashi

Doctoral Program in Fundamental Sciences  
Graduate School of Science and Technology

Niigata University

## **Abstract**

Crystallographical and micro-textural information of accessory minerals have not been applied widely to petrology although they occur commonly in various rocks. In this study the two accessory minerals, thorite and zircon from Cape Ashizuri Ring Complex, Kochi, SW Japan were mineralogically described mainly by transmission electron microscopy (TEM) and scanning electron microscopy (SEM). In thorite mineralogy, thermal behavior of the metamict state in nano-scale was investigated experimentally and the results suggested a possibility of application to a kind of geochronology. In zircon mineralogy, unusual internal textures of zircon were newly found by cathodoluminescence (CL) method and new perspective to magmatic process are suggested. These crystallographical/textural characteristics were very important for application of these accessory minerals in geochronology and petrology.

# Contents

<b>Abstract</b> .....	1
<b>Introduction</b> .....	3
<b><u>Chapter 1: Thorite</u></b>	
Abstract .....	4
1. Introduction .....	5
2. Samples and geological background .....	6
3. Experimental procedure .....	7
4. Results	
4.1 Thorite from Cape Ashizuri Ring Complex .....	8
4.2 HRTEM observations for annealed samples .....	8
5. Discussion	
5.1 The structural unit of metamict thorite .....	13
5.2 Comparison with previous results .....	13
5.3 Kipawa syenite complex .....	14
5.4 The 5 m.y. evidence from the metamict state .....	16
6. Conclusions of Chapter 1 .....	18
<b><u>Chapter 2: Zircon</u></b>	
Abstract .....	19
1. Introduction	
1.1 The petrogenesis of A-type granite .....	20
1.2 Cape Ashizuri Ring Complex .....	20
1.3 Various internal textures and chemical features of zircon .....	23
2. Sample descriptions .....	25
3. Analytical methods .....	28
4. Results	
4.1 Internal textures of zircon from Cape Ashizuri Ring Complex .....	29
4.2 Chemical features of each internal texture – quantitative point analysis .....	35
4.3 Chemical features of each internal texture – qualitative mapping analysis .....	38
5. Discussion	
5.1 Formation mechanism of the secondary internal textures .....	40
5.2 Growing sequence of the internal textures .....	42
5.3 Zr-undersaturation event .....	45
5.4 Melt compositions around Zr-undersaturation event .....	49
5.5 Discrete development of two magmas .....	49
6. Conclusions of Chapter 2 .....	52
<b>Conclusions</b> .....	53
<b>Acknowledgments</b> .....	53
<b>References</b> .....	54

## **Introduction**

Accessory mineral have studied for a long time and a part of them have applied for petrology as very important tools. However, a large number of mineralogical reports about accessory minerals are still remained just as “mineralogical” knowledge, not applied for geology or petrology.

Crystallographical and micro- (or nano-) textural knowledge of mineral is the typical instance. One of that, for example, metamictization is most characteristic nature of radioactive minerals and many crystallographical/nano-textural results have reported by mineralogists and material scientists; however the time-dependency of metamictization is still not applied in any geological aspect. In another case, zircon secondary internal textures which have studied for two decades are currently starting to apply as petrological tool (e.g. Grant et al., 2009; Claiborne et al., 2010).

Zircon is now one of the most important accessory mineral; and other than zircon, igneous rocks (especially felsic one) often include the minerals which have strong/intermediate radioactivity, such as monazite, xenotime and thorite. This study presents a possibility of applying these crystallographical and micro/nano-textural results to geochronology and petrology.

# Chapter 1: Thorite

## Abstract

Thorite ( $\text{ThSiO}_4$ ) occurs frequently at Thorium deposit and is commonly found as metamict state. However, most studies about metamictization have been carried out on zircon. Less crystallographic examination of thorite which is isomorphous with zircon has been done. Although metamictization is well known, there has been no applicational trial of metamictization phenomena to interpretation of geologic process and geochronology. The thermal behaviors of nanotextures of metamict thorite were examined by HRTEM, using samples from Ashizuri-misaki ring complex.

At  $850^\circ\text{C}$  and  $1000^\circ\text{C}$ , metamict thorite forms characteristic granular nanotextures that consist of thorianite nanocrystals and amorphous silica. The electron diffraction (ED) patterns of unheated thorite and the nanocrystals implicate that the nearly amorphous state of metamict thorite consists of the structural unit of  $\text{ThO}_8$  regular hexahedron. Halo-like ED pattern of metamict thorite represents the minute aggregate units which are composed of a few unit cells of thorianite.

Analogous granular nanotexture was reported for natural zircon and thorite (Meldrum et al., 1999). The formation of the granular nanotexture requires complete metamict state in the mineral prior to heating. So, it requires the term for finishing the metamictization between crystallization by heating in order to form such granular nanotexture in natural. This principle may allow applying thorite and other metamict minerals as the geochronological tool to specify the time-lag between crystallization and thermal event or multiple thermal events.

## 1. Introduction

It is well known that radioactive mineral becomes metamict state after a certain period. Those minerals and analogous phases are more important in relation to treatment of nuclear waste (Ewing, 2001; Carrez et al., 2003; Mishra et al., 2007; Seydoux-Guillaume et al., 2009, Lian et al., 2009).

One of well known metamict minerals is zircon ( $\text{ZrSiO}_4$ ) and many studies of metamictization have been carried out on zircon (e.g. Murakami et al., 1991; Salje et al., 1999; Nasdala et al., 2002). On the other hand, the studies dealt with the other metamict minerals have not been studied in more detail, even in the minerals which isostructural with zircon, thorite ( $\text{ThSiO}_4$ ) and coffinite ( $\text{USiO}_4$ ).

Meldrum et al. (1998, 1999) and Lian et al. (2009) studied on those minerals by transmission electron microscopy (TEM) with ion-irradiation, the common technique for revealing amorphization process and related properties. However, most studies including those of Meldrum et al. (1998, 1999) and Lian et al. (2009) have been done about the metamictization process and radiation resistance of the minerals. Detailed metamict states of those minerals containing short-range structural characterization have not been examined; especially other than zircon (structural analyses of metamict zircon have been carried out using X-ray diffraction (XRD) analysis; e.g. Vance and Anderson, 1972).

Few studies of e.g. Farges and Calas (1991) focused on structure of short-range ordering in natural metamict thorite and reported an interesting EXAFS data. They described that the Th atom site in thorite maintains constant atomic distance from the nearest O atom even in a completely metamict state, unlike the Zr atom site in zircon. They concluded that the eight-fold coordinate  $\text{ThO}_8$  dodecahedron in crystalline thorite retains the same coordination number even after metamictization is finished.

There are some thermal annealing studies on thorite to speculate the crystal state through the thermal behavior. These studies presented the generation of thorite, huttonite ( $\beta\text{-ThSiO}_4$ ) and thorianite ( $\text{ThO}_2$ ) crystals by annealing of metamict thorite (Pabst, 1952; Harris, 1959; Hayashi et al., 1969). All those studies used XRD method for identifying the crystal phases and little knowledge about the textures were obtained and formation mechanism of annealed thorite has not been discussed. This chapter presents the crystallographic description of natural metamict thorite and its annealing-caused nanotexture by TEM and short-range structure of metamict mineral and its thermal behavior will be discussed.

## 2. Samples and geological background

In this study, thorite was selected as metamict mineral from the following reasons; (1) comparable to zircon study (originally isostructural with zircon), (2) metamictize shortly (within several Ma) after the crystallization, (3) occasionally crystallizes igneously (presents as an accessory mineral) and in that case it is easy to estimate the post-crystallization event, (4) relatively much data are available than coffinite, and (5) interesting remark has already been given by Farges and Calas (1991). Thorite sample used in this study was collected at Cape Ashizuri Ring Complex in Kochi, SW Japan.

Cape Ashizuri Ring Complex (10-16 Ma, obtained by Rb-Sr, K-Ar and zircon FT age determination) is an intrusive unit that penetrates into the paleogenic Shimizu group belonging Shimanto accretionary zone. The ring complex is composed of six plutonic lithofacies with four intrusive stages and two other dykes (Murakami and Imaoka, 1980; Murakami et al., 1983, 1989; Murakami and Masuda, 1984; Imaoka et al., 1991). Murakami et al. (1989) supposed a model suggesting that the intermissive intrusion of magmas occurred within a short term. Most of the plutonic rocks are massive and any metamorphic evidences are not reported in each lithofacies.

I found green thorite as an accessory mineral from the two rock samples (quartz syenite and coarse biotite granite) of Cape Ashizuri Ring Complex. However, no significant difference was observed between those thorite grains on crystallinity, chemical composition and thermal behavior. Similar thorite reported by Hayashi et al (1969) at the placer deposit in the region. Separated thorite grains are 100-200  $\mu\text{m}$  long, transparent green in color and generally translucent. It shows a euhedral short prismatic shape with {101} and {100} planes. The rock samples are homogeneous and remain unaltered, thus the accessory minerals including thorite are identified as igneous origin.

### 3. Experimental procedure

Rock samples were crushed by a jaw crusher and passed 80 mesh. After heavy liquid and magnetic separation, the target mineral was hand-picked from the residue under a binocular microscope. Bromoform and methylene iodide were used for heavy liquid separation and a neodymium magnet and a Frantz Isodynamic Separator were used for magnetic separation.

The annealing experiment was conducted at 700°C for 48 h, 850°C for 4 h, 850°C for 48 h and 1000°C for 12 h. Sample grains in a porcelain crucible were heated in air using a muffle furnace (ADVANTEC, FUW220PA).

Nanotextures were observed using TEM (JEOL, JEM-2010, 200kV). Samples for TEM observations were prepared by crushing method. Finely crushed fragments were placed on a carbon-coated, porous triafol film on a Cu mesh. I did not apply the ion milling method in view of the risk of confusing artificial amorphous layer with the original metamict state. High-resolution TEM (HRTEM) images and selected area electron diffraction (SAED) patterns are obtained from each TEM samples. I confirmed that the influence of electron irradiation on sample crystallinity is negligible through continuous irradiation of strong electron-beam for 2 h. The Fourier filtering of the TEM image is carried out using the ImageJ image processing and analysis program (available at <http://rsbweb.nih.gov/ij/>). Chemical analyses (point analysis and elemental mapping analysis) were carried out for some samples by energy dispersive X-ray spectroscopy (EDS).



## 4. Results

### 4.1 Thorite from Cape Ashizuri Ring Complex

The SAED pattern of the natural sample (thorite from Cape Ashizuri Ring Complex) does not show diffraction spots but does show a halo pattern (Fig. 1). No heterogeneity was found in HRTEM observations at magnifications of 40,000 to 500,000. There is no peak corresponding to  $d(101)$  in the SAED pattern. 69.9 wt% of Th, 10.4 wt% of Si, 15.2 wt% of O and 4.6 wt% of U was detected by semi-quantitative EDS analysis. Consequently, it is obvious that the natural sample is identified as thorite by its chemical composition and crystal form. It has fully metamict state.

### 4.2 HRTEM observations for annealed samples

#### *700°C - 48 hours*

The SAED pattern of the sample annealed at 700°C for 48 h is quite similar to that of untreated natural thorite (Fig. 2a). However, the HRTEM image shows nanodomains as the ordered assemblage of four to ten unit cells in a region 1-2 nm across, respectively. The difference from the natural sample is quite obvious on both the HRTEM image and the Fourier filtering image (Fig. 3a). The inner halo of the SAED pattern represents approximately 3.2 Å of  $d$ -value and it would correspond to the lattice width of the nanodomains.

#### *850°C - 4 hours*

The SAED patterns of most of the samples annealed at 850°C for 4 h remained unchanged from the natural thorite. However certain regions show one or more crystalline part of approximately 5 nm in diameter and the corresponding SAED pattern has a spot in the inner halo-ring (approximately 3.2 Å). The shape of the crystalline part is irregular and it tends to densely-distributed at particular region (Fig. 2c).

The SAED pattern becomes to be close to spotty ring at the dense zone of the crystalline part. The mineral phase of the crystalline part is identified as thorianite from its  $d$ -value of 3.2, 2.8, 2.0 and 1.7 Å.

#### *850°C - 48 hours*

The sample annealed at 850°C for 48 h shows an SAED pattern of an entirely spotty ring (Fig. 2d). A lot of crystalline parts are observed on the HRTEM image, but their size (approximately 5 nm) remain mostly unchanged from the sample annealed at 850°C for 4 h.

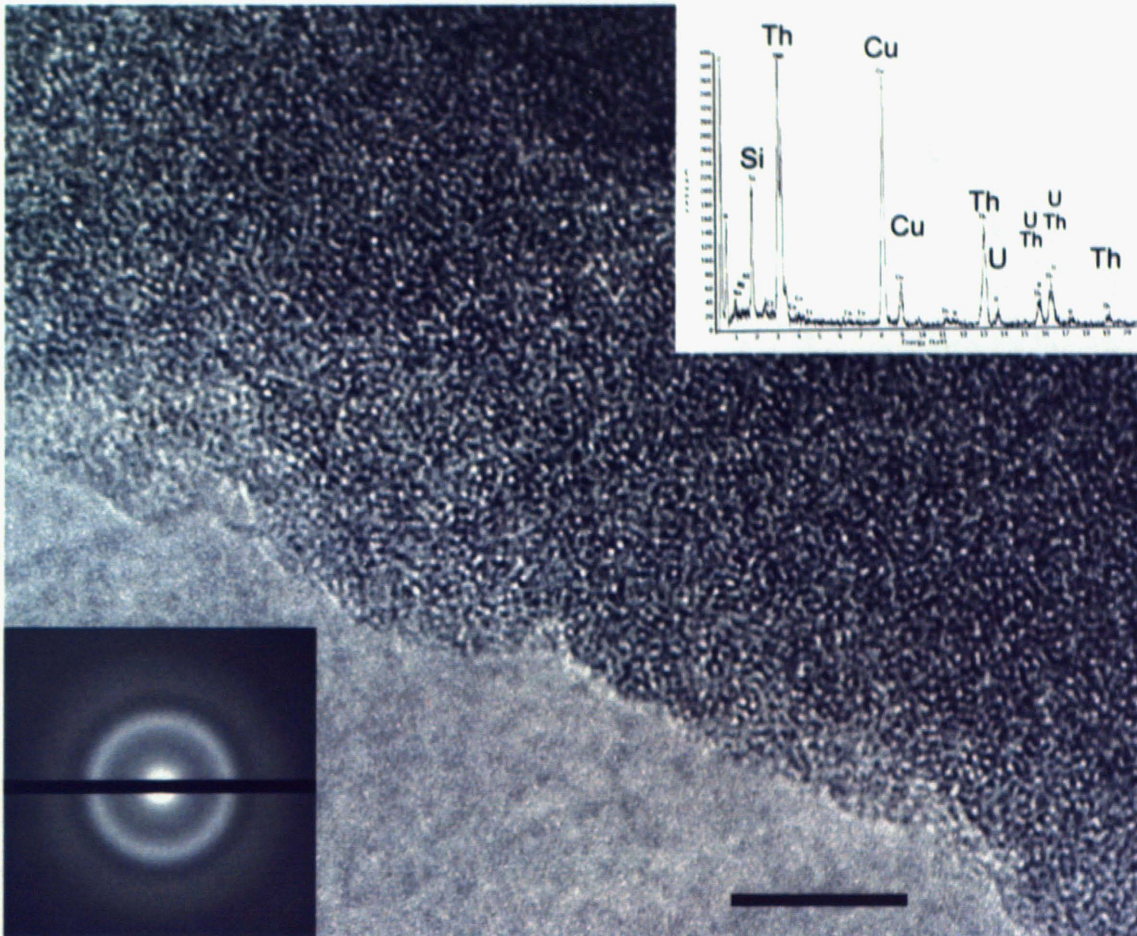


**Fig. 1.** HRTEM images of thorite from Cape Ashizuri. Electron diffraction pattern (bottom left) and the spectra of EDS point analysis (top right) have been inserted. The scale is 5 nm. Cu peak in EDS pattern is due to the sample-supporting Cu mesh.

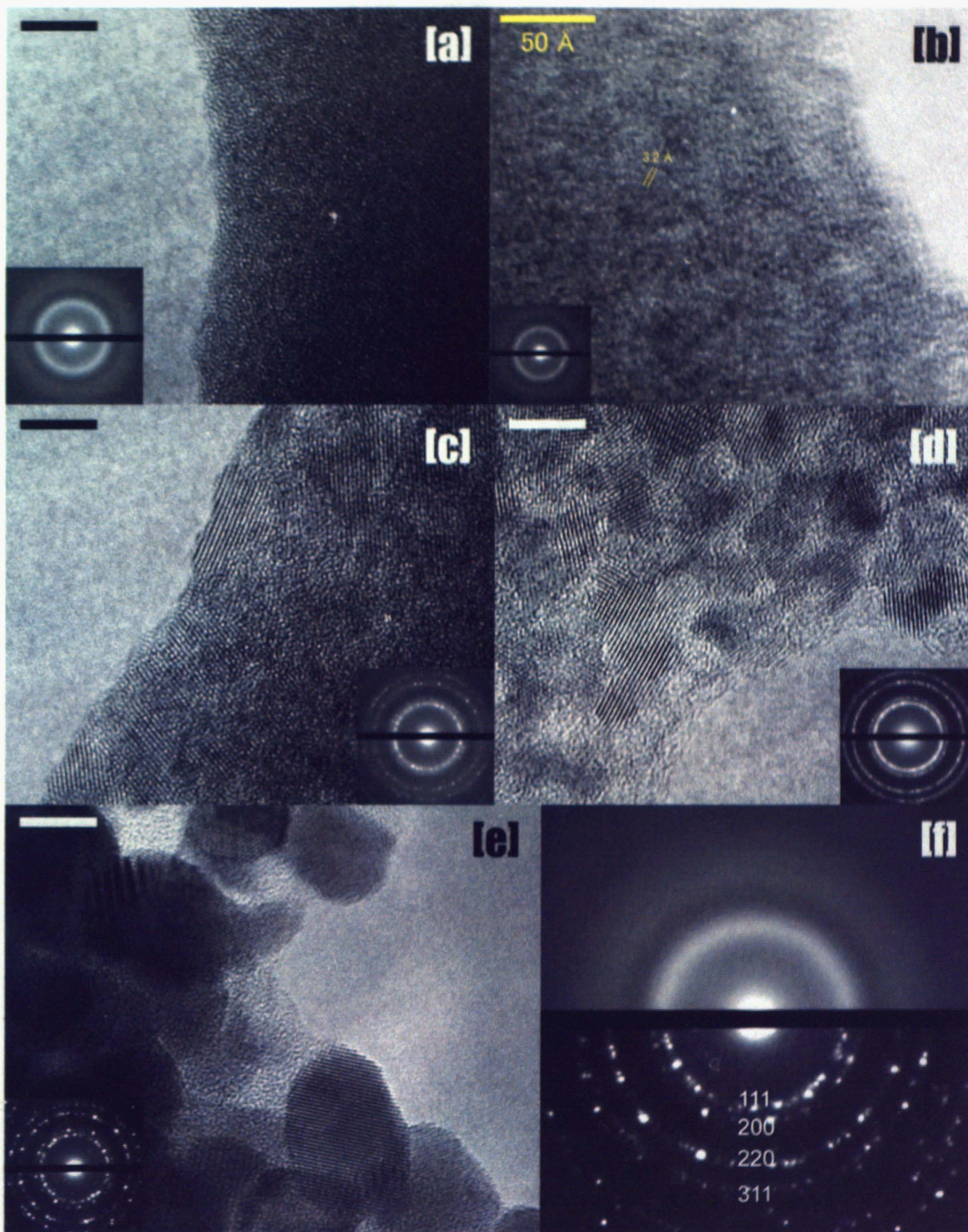


**Fig. 2.** HRTEM images of annealed metamict samples: (a) 700°C at 48 h, (b, c) 850°C at 4 h, (d) 850°C at 48 h and (e) 1000°C at 12 h. Corresponding electron diffraction pattern has been inserted. The scale is 5 nm. A comparison of the electron diffraction patterns of natural thorite (top) and samples annealed at 1000°C for 12 h (bottom) is shown in (f). See text for details.

### ***1000°C - 12 hours***

The SAED pattern of the sample annealed at 1000°C for 12 h (Fig. 2e) is much spottier than the sample annealed at 850°C for 48 h. The thorianite nanocrystals have enlarged to 10-15 nm in diameter and clearly show grain shapes. Each nanocrystal is randomly oriented, and no heterogeneity was observed in those grain size and grain shape.

TEM-EDS elemental mapping was carried out for Th, U and Si on this annealed sample (Fig. 3b). The result indicates that the nanocrystals are certainly thorianite and the amorphous matrix is composed not of ThSiO<sub>4</sub> but mainly of SiO<sub>2</sub>.

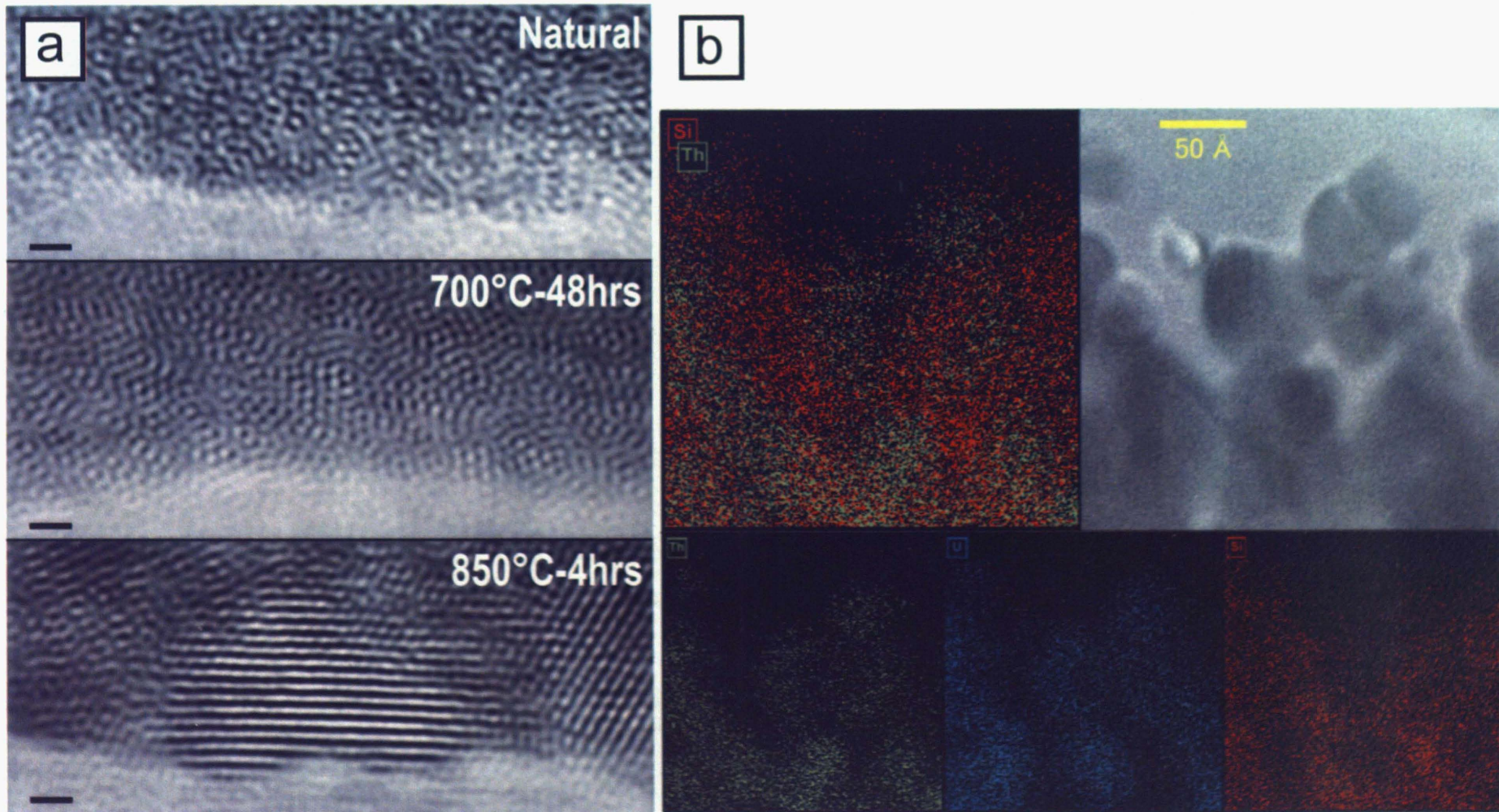


**Fig. 3.** (a) Fourier filtering images of samples annealed at 700°C for 48 h, 850°C for 4 h and natural thorite. There is almost no difference in electron diffraction patterns between natural thorite and the sample annealed at 700°C (Figs. 2 and 3a). However, the latter shows domains composed of a few unit-cells arranged in the HRTEM image. The crystalline parts in the 850°C annealed sample are thorianite. The scales are 1 nm. (b) TEM-EDS elemental mapping image of a sample annealed at 1000°C for 12 h. There is a contrasting distribution of Th and Si.

## 5. Discussion

### 5.1 The structural unit of metamict thorite

I obtained two types of SAED pattern in TEM observation; well-known halo patterns (natural sample and sample annealed at 700°C) and spotty ring patterns (samples annealed at 850°C and 1000°C). However these patterns have same d-values which correspond to thorianite (Fig. 2f), and then the substantive difference of them must correspond to the degree of peak broadening causing crystal smallness (e.g. Cawley, 1992). One of the evidence is correlation between enlargement of the crystalline part (Fig. 3a) and sharpening of the SAED pattern, both as the annealing temperature increase.

Consequently, I identify the structural unit of metamict thorite as thorianite unit cell. This is not the same thing as metamictization-induced “anti-glass” state (Redfern, 1996), because metamict thorite has the d-values of thorianite on the SAED pattern, instead of that of the crystalline remnant of thorite. Hence, the “thorianitic” structural unit must not be the same with crystalline remnant of thorite structure but correspond to the final product of thorite metamictization (see also next section).

A change of the crystallinity from fully metamict state (natural sample) to nanodomains (sample annealed at 700°C) would be explained as structural relaxation (e.g. Feltz, 1993). It means that the “metamict” state of thorite is apparently unchanged from natural state up to 700°C annealing (at least SAED and probably XRD analyses), but the nano-scale crystal state is not constant with the annealing temperature and the time since annealing. The former is derived from the various degree of structural relaxation which corresponds to the annealing temperature and the latter is caused by the restart of metamictization after annealing.

### 5.2 Comparison with previous results

The present results suggest that the thermal behavior of metamict thorite is quite similar to that of zircon (e.g. Vance and Anderson, 1972); with one difference that metamict thorite shows only one d-value set of *c*-ThO<sub>2</sub> (thorianite) through the thermal annealing (whereas *t*-ZrO<sub>2</sub> and *m*-ZrO<sub>2</sub> along with *c*-ZrO<sub>2</sub> have reported on zircon).

On the other hand, some differences from previous thorite study (Pabst, 1952; Hayashi et al., 1969) are found; the present results have no crystalline phase of thorite and huttonite, in addition neither previous study described the thorianite-dominant state. These differences may be caused by difference in the starting thorite and/or the annealing conditions.

Farges and Calas (1991) concluded through their EXAFS study that the Th-O interatomic distances and Th-coordination numbers of crystalline thorite remain at the same value; even in the metamictization was completed. However I think that there may

be a risk of misinterpretation in their description; there was little mention of the two types of Th-O distances in ThO<sub>8</sub> dodecahedron of thorite structure. Those distances are clearly different, 2.37Å and 2.47Å, but its average distance 2.42Å is accidentally same with the Th-O distance of thorianite structure.

As discussed above, the present results imply “thorianitic” structural units in metamict thorite. Thus, in my interpretation, ThO<sub>8</sub> dodecahedron of thorite structure would be decomposed through metamictization and the two Th-O distances are not remaining with pristine value (but had unified “thorianitic” Th-O distance, 2.42 Å).

### 5.3 Kipawa syenite complex

A nanotexture similar to the thorianite nanograins in this study has been reported in natural sample. Meldrum et al. (1999) described the distinctive nanotexture consisting of granular nanocrystals and an amorphous matrix in natural zircon (from Sri Lanka) and thorite (from Kipawa, Canada).

In reference to this study’s annealing results, it would be remarkable to find this nanotexture in nature; however, there seems to be just one significant misinterpretation in their description. Meldrum et al. (1999) found granular nanocrystals in the Sri Lankan zircon, and they also noted that the electron diffraction pattern corresponds to zircon. I think latter description is rather suspicious; because the SAED pattern of the nanotexture is quite similar to that of the *c*-ZrO<sub>2</sub>, which is observed in the same paper (Fig. 4). Additionally, to identify the SAED pattern of the nanotexture they adopted four indices; (110), (200), (102) and (121), however, the indices of the electron diffraction ring seem to be incorrectly interpreted.

Assuming that the HRTEM image and corresponding SAED pattern in Meldrum et al. (1999) was correct, the nanocrystals should correspond to *c*-ZrO<sub>2</sub> (at zircon from Sri Lanka) or thorianite (at thorite from Kipawa). Those nanotextures may form by heating the metamict state, according to the results of this study’s annealing of metamict thorite.

The Kipawa syenite complex, which included the thorite of Meldrum et al. (1999), shows amphibole porphyroblast and microscopic metamorphic texture in each lithofacies (Currie and van Breemen, 1996; van Breemen and Currie, 2004). Therefore, if the nanocrystal was thorianite and it was formed by a thermal event such as metamorphism, the thorite grain must have been fully metamictized (Stage III in Murakami et al., 1991) at the time when the syenite complex was heated.

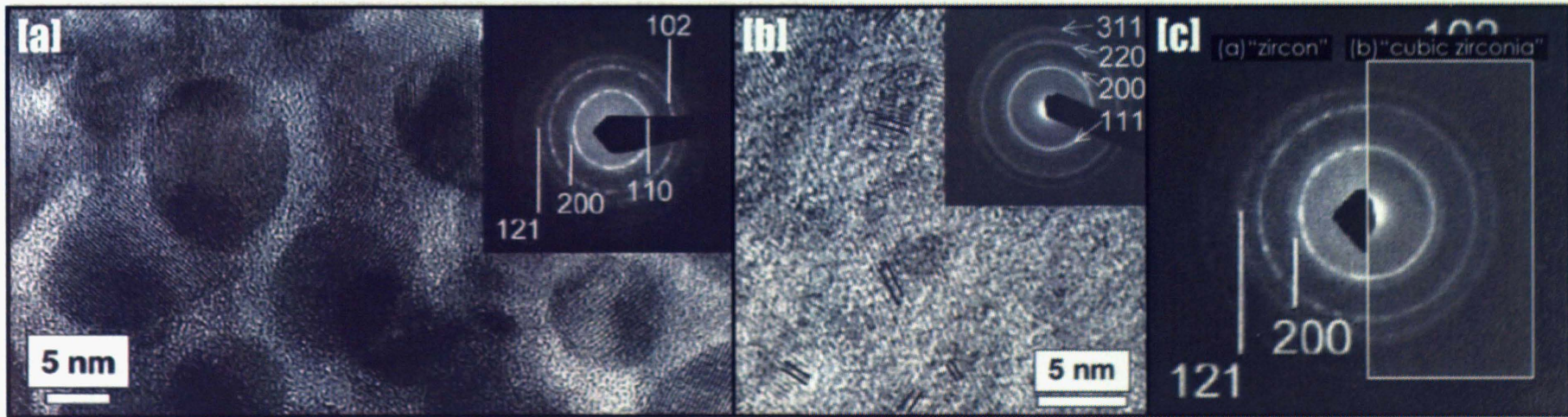


**Fig. 4.** HRTEM images of (a) Sri Lankan zircon and (b) cubic zirconia which was formed by ion-beam irradiation to zircon at 800°C. The corresponding electron diffraction patterns have been inserted and are compared in (c). Figures (a) and (b) are after Meldrum et al. (1999). They concluded that the crystalline parts of (a) correspond to zircon and the crystalline parts of (b) correspond to cubic zirconia; however, there is a significant coincidence between those two electron diffraction patterns (c). The indices described in (a) are inconsistent with known data of zircon in both the proportion of d-values and the intensity distributions.



#### 5.4 The 5 m.y. evidence from the metamict state

According to the calculation by Meldrum et al. (1999), pure thorite crystal requires a term of 5 m.y. for complete metamictization. The fact that young Cape Ashizuri Ring Complex (10-16 Ma) includes completely metamictized thorite are also consistent with their calculation. That is, the occurrence of thorianite nanograins at the Kipawa syenite complex ensures a blank period of 5 m.y. between the intrusion (accurately cooling of crystallized thorite below the annealing temperature) and the metamorphic event (Fig. 5). Whereas thorite crystal completes the metamictization through 5 m.y., thorianite crystal is confirmed to be barely metamictized as a result of the self-annealing property (Seydoux-Guillaume et al., 2009), as with uraninite (Janeczek et al., 1996).

The 5 m.y. blank-period evidence is, of course, applicable to other similar occurrences with the Kipawa syenite complex, and the same principle is also applicable to metamict minerals other than thorite (e.g., zircon and other zircon group minerals). When we try to apply the principle to minerals other than thorite, the period from crystallization to complete metamictization should be considered carefully; it varies with each mineral composition (radioactive elements in the main components or impurities) and each crystal structure. The metamictization period is empirically known as 5 m.y. for thorite and in the range of 0.1 to 1 billion years for zircon (Palenik et al., 2003). According to Murakami et al. (1991), the complete metamictization of zircon from crystalline to the fully metamict state requires an  $\alpha$ -decay event dose of  $8 \times 10^{15}$   $\alpha$ -decay events/mg. Then we can achieve a cumulated dose from the content of  $^{238}\text{U}$ ,  $^{235}\text{U}$ ,  $^{232}\text{Th}$  and the age of the sample (Holland and Gottfried, 1955).

However, in order to use this principle, a thermal metamorphic rock containing metamict mineral is required. Thorite is often used to be missed in petrographic descriptions; in fact there are few instances of thorite being found as an accessory mineral. I think the reasons why thorite is not properly described may be as follows: zircon and thorite are very similar under polarizing microscope; furthermore, thorite had been considered to be less significant mineral in petrology (in recent days, latter is not entirely true because of prevailing CHIME dating). I have found unreported thorite as an accessory mineral of four granitoids in Japan, including the sample used in the present study (Cape Ashizuri, Kochi; Iwafune, Niigata; Hane-gawa, Niigata; Takase-gawa, Nagano).

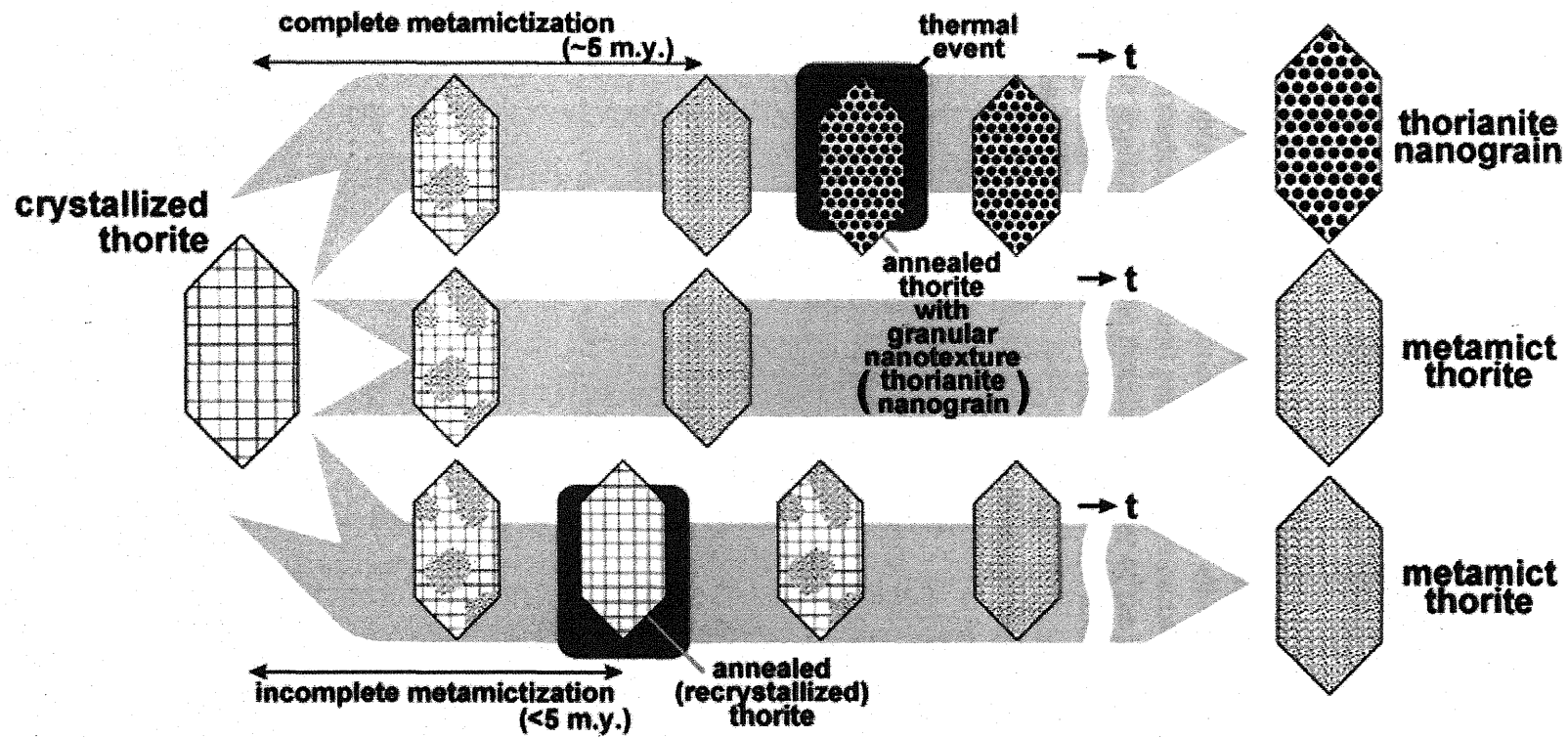


**Fig. 5.** Model figure suggesting the principle of 5 m.y. evidence based on thorite metamictization. Thorianite nanograins are formed in thorite grain by heating after complete metamictization (top). It has been confirmed that little metamictization occurs in thorianite, even throughout the geological timescale (Seydoux-Guillaume et al., 2009). On the other hand, thorite, which contains a remaining crystalline part, is considered to recover the original crystal structure when it undergoes heating (bottom). The recovered thorite crystal will have re-metamictized over the next 5 m.y. In that case, the eventual thorite grain will show no evidence of a thermal event (bottom right) in comparison with the thorite grain which has undergone no thermal event (middle right).

## 6. Conclusions of Chapter 1

- (1) Thorite was newly found at two lithofacies of Cape Ashizuri Ring Complex in SW Japan. The thorite was mineralogically described mainly by TEM with special reference to its metamict state.
- (2) A heating experiment of the metamict thorite was conducted at temperatures between 700°C to 1000°C in air. HRTEM observations and EDS analyses of the samples showed nanotextures consisting of thorianite nanocrystals and amorphous silica.
- (3) The electron diffraction patterns of the metamict thorite and thorianite nanocrystals indicated that a  $\text{ThO}_8$  regular hexahedron is the structural unit of metamict thorite. Both the natural sample and sample annealed at 700°C show a halo-like electron diffraction pattern corresponding to a few unit cells of 1-2 nm across.
- (4) A possible application of the thermal behavior of the metamict thorite nanotexture to geochronology was discussed on the basis of the analogous nanotexture previously reported in natural samples.

## Chapter 2: Zircon

### Abstract

Various internal textures of zircon from Cape Ashizuri Ring Complex, Kochi, SW Japan were newly found and described by scanning electron microscope (SEM) and cathodoluminescence (CL) observations. The chemical features including  $\text{HfO}_2$ ,  $\text{Y}_2\text{O}_3$ ,  $\text{UO}_2$  and  $\text{ThO}_2$  were also described.

Unusual internal textures of the zircon are classified into three types: Resorption Disturbance texture (RD), Local Disturbance texture (LD) and Hafnon-like Disturbance texture (HD). RD is cutting a part of original oscillatory zoning with rounded boundary and is interpreted to be resorption-precipitation texture. LD is divided into two subtypes, LD1 and LD2: LD1 is developing at core and showing dendritic shape; on the other hand, LD2 is also developing at rim and closely related to melt inclusions. The chemical features indicate that LD corresponds to local recrystallization texture. HD is developing from zircon surface toward core deeply and accompanied by LD2. It has characteristically high concentration of  $\text{HfO}_2$ , so HD would have been formed in Hf-rich post- or late-magmatic fluid phase like hafnon. Through the SEM observation, six growth stages of the zircon including these secondary internal textures are suggested as follows: (1) igneous or hydrothermal core, (2) LD1, (3) RD, (4) igneous rim with enclosing melt, (5) LD2 around the melt inclusions and (6) outermost igneous rim.

RD indicates  $\text{ZrSiO}_4$ -undersaturated environment, however all the other minerals from the Ring Complex except zircon have no record of such compositional change of the melt. I suggested three possible cases as the magmatic event based on zircon internal textures; (1) inflow of high temperature magma which is associated with a compositional shift, (2) addition of volatile fluid probably rich in fluorine and (3) transient solidification and subsequent fractional melting. RD and LD2 are observed in many zircons that have different compositions and are included in different lithofacies. Therefore, the different magma generation and similar magmatic development are strongly suggested for two lithofacies of Cape Ashizuri Ring Complex.

## **1. Introduction**

### **1.1 The petrogenesis of A-type granite**

A-type granite, which is defined by Loiselle and Wones (1979), is characterized as the alkalic bulk composition of the rock. It also has highly-concentrated trace elements including F, Zr, Ga, Nb, Y and REEs, and on another front it has low concentrations of CaO and H<sub>2</sub>O. The word “A” is originally defined as “Anologenic” in Loiselle and Wones (1979), which depends on the common occurrence, so the term “A-type” is not directly representing the magmatic origin unlike other classification terms such as I-type and S-type in granite petrology. Bonin (2007) suggested a suspicious expression to the term “A” that the term really means the “Alkaline”, “Anhydrous”, “Aluminous” chemical features or the “Ambiguous” origin.

So far, many researchers have tried to reveal the origin of A-type granite magma; however the consensus has not been achieved yet. Loiselle and Wones (1979) presented the fractionation model which is described as fractionation or assimilation of alkali basaltic magma at lower crust and its intrusion with minor or no contamination of middle and upper crust, that is caused by the uprising magma passes through an extensional crack.

On the other hand, several investigators are supporting metasomatic model. It regards the alkalinity was derived from F- or CO<sub>2</sub>-rich fluid phase which had added to the system during or after the intrusion (Taylor et al., 1980; Bonin, 1982; Bowden and Kinnaird, 1984).

Collins et al. (1982) and other workers (e.g. Clemens et al., 1986) argued that A-type magma had been generated by the partial melting of anhydrous lower crustal rock, which corresponds to the residual rock which had previously generated I-type granitic magma. There are also other suggestions including the hybrid model of above instances (e.g. Martin, 2006), however almost all models have based on each occurrence (cf. Nigerian Younger granites at Loiselle and Wones, 1979 and Australian A-type stocks associated with I-type batholithes at Collins et al., 1982) and no model achieved general agreement.

### **1.2 Cape Ashizuri Ring Complex**

Cape Ashizuri Ring Complex, Kochi, SW Japan, which is composed of mainly alkalic plutonic rocks with five intrusive stages, and it is the only A-type granite in Japan. The ring complex had studied in 1980s mainly by Dr. Murakami; they have made achieved following knowledge (Fig. 6; Murakami and Imaoka, 1980, 1985; Murakami et al., 1983, 1989; Murakami and Masuda, 1984; Iizumi and Murakami, 1985; Imaoka et al., 1991).

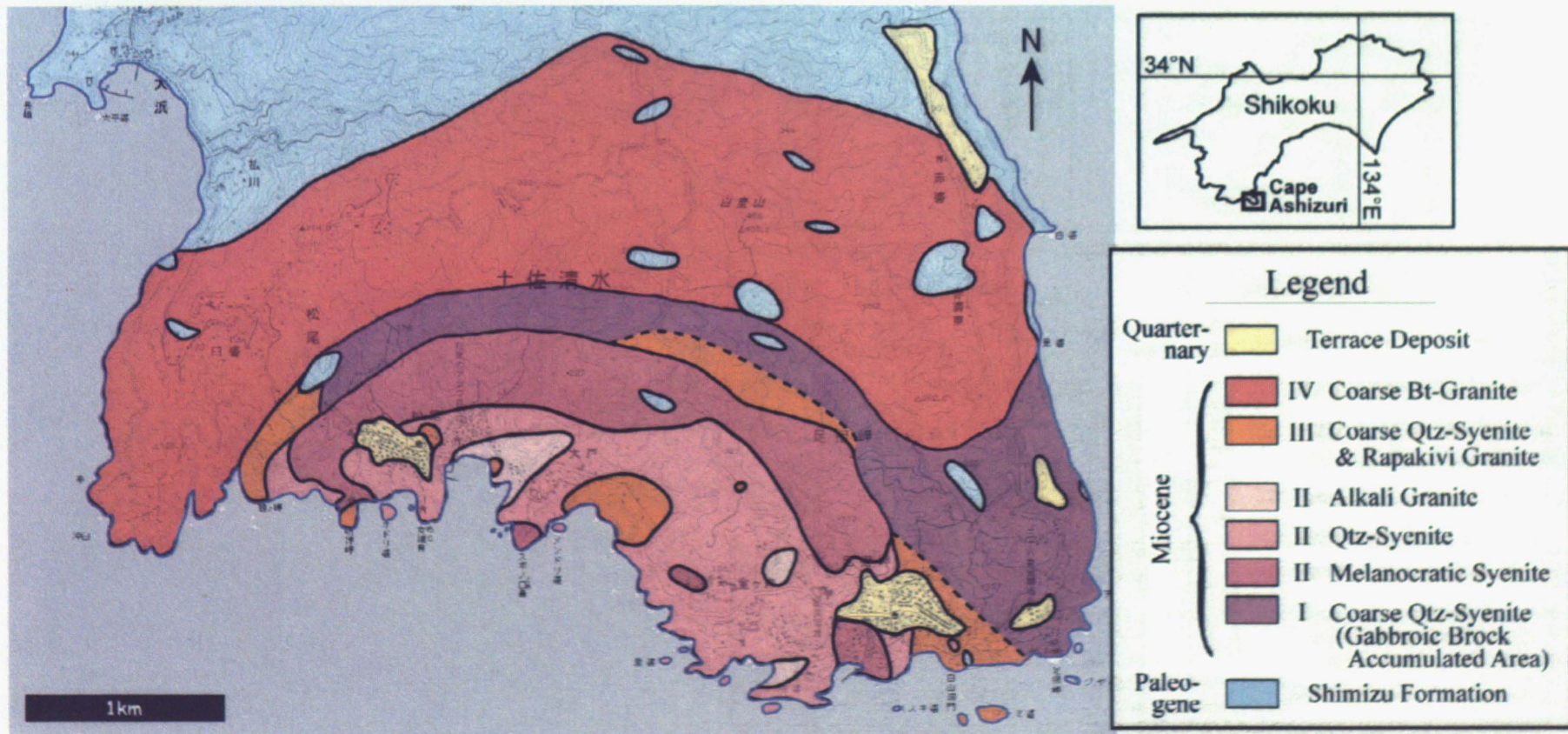


Fig. 6. Geological map of Cape Ashizuri Ring Complex, modified after Murakami and Masuda (1984). Dykes are omitted. The roman numbers in legend are intrusion stage (see text in detail).

The constituent lithofacies are follows: coarse quartz-syenite (gabbroic blocks densely accumulated part; stage I), melanocratic syenite (stage II), quartz-syenite (stage II), alkali granite (stage II), coarse syenite and rapakivi granite (stage III), coarse biotite-granite (stage IV), aplite and granophyre (stage IV), alkali dolerite and syenite porphyry (stage V). The latter two facies (aplite and granophyre of stage IV and alkali dolerite and syenite porphyry of stage V) are all occurs as dikes. Alkali feldspar is observed in all lithofacies except stage I, and also high modal ratios of alkali feldspar than plagioclase are seen in almost all acidic rocks. Clinopyroxene (stage I, II and V), hornblende (stage I to V) and biotite (stage II to V) are included as mafic minerals. Most of igneous rocks are nearly massive and not show flow structure, with the exception of stage III lithofacies.

These igneous rocks intruded into paleogenic Shimizu formation, which is mainly composed of sandstone and shale. The shale in Shimizu formation is also found as roof pendants of the ring complex.

The ring complex had intruded at 10-16 Ma; the age data were derived by the radiometric dating of K-Ar hornblende, biotite and whole-rock age (Shibata and Nozawa, 1968; Murakami et al., 1989), Rb-Sr whole-rock age (Iizumi and Murakami, 1985) and zircon fission-track age (Murakami et al., 1989). The magmas seem to have intruded one after another; because no thermal metamorphism is confirmed in these lithofacies. In contrast the Shimizu formation had been undergone heating and partly forming biotite-hornfels.

All lithofacies of the ring complex have high concentrations of Na<sub>2</sub>O, K<sub>2</sub>O, F, Zr, Ga and REE and also low concentrations of CaO and H<sub>2</sub>O. From this bulk-rock chemistry, these acidic rocks are classified into A-type granite. It is considered that the strongest chemical features of A-type granite are seen in stage II rocks and some contaminations from upper crustal material are recognized in stage IV coarse biotite-granite (the latter consideration was derived by the relatively high Sr initial ratios). However, A-type granites are regarded as being commonly seen in rift zones and stable cratons, so the occurrence of this kind of granite at subduction zone is quite rare (Best and Christiansen, 2001; Bonin, 2007).

Murakami et al. (1989) estimated that the chemical features of the ring complex are similar to Nigerian granitoids of Loiselle and Wones (1979). Therefore, they took the magmatic evolution of the ring complex as same with the Nigerian case. Thus, Murakami et al. (1989) has an assumption that there was a huge extensional crack which reaches to lower crust; however they also posed the question what mechanism had formed the crack. This area, Cape Ashizuri, is typical compressional field which has dominant accretionary prism of Shimanto belt and would not be easy to form such extensional crack.

In addition to the question, Murakami et al. (1989) provided little explanation for the question why this A-type granite occurs at subduction zone. They estimated the magmatic origin of the ring complex mainly from bulk-rock chemical features and similarity of those with Loiselle and Wones (1979); accordingly there is lack of the mineral textural evidence which directly indicates the magmatic events.

### 1.3 Various internal textures and chemical features of zircon

#### *Internal textures*

Zircon ( $ZrSiO_4$ ) is widely used for U-Pb dating because of the widespread distribution and the thermal and chemical durability. Zircon also has zonal structure and/or various secondary internal textures which are resulted from different growing condition respectively; hence recently it is noticeable as a record of the growth environments especially various stages of high-grade metamorphism (e.g. Wu et al., 2006; Orejana et al., in press). This chapter will describe the various internal textures of zircon from Cape Ashizuri Ring Complex and achieve a good suggestion of the magmatic evolution from the internal textures and surrounding data.

Internal textures in zircon grains are commonly observed using Scanning Electron Microscopy (SEM) with the detector of Back-Scattered Electron (BSE) or Cathodoluminescence (CL). For detailed observation of internal texture CL image is preferentially used. The other method is BSE image; difference of impurity contents is easily found within the same crystal. Since 1990s, many zircon crystals have been observed by SEM as CL detector and many studies of zircon internal texture have been reported (e.g. Vavra and Hansen, 1991; Nemchin et al., 2001; Corfu et al., 2003).

Igneous zircon commonly has two-type internal texture; one is a sharp, polygonal and concentric zonal structure which is called as “oscillatory zoning”, and the other is “sector zoning” which are also called as “hour-glass structure”. The former reflects the various impurity components among a band and other band; it is originally formed by the multiple growth stages and perhaps liesegang phenomenon (Hoskin, 2000). The latter, sector zoning is formed by the different growth rates among each crystal plane (e.g. Watson and Liang, 1995).

On the other hand, hydrothermal (including pegmatitic) zircon has clearly different internal texture from igneous zircons; it has numerous microscopic inclusions and therefore it shows “spongy” internal texture in whole (e.g. Hoshino and Ishihara, 2007). Hydrothermal zircon also has high BSE emission which resulted from the high concentration of impurities.

Unlike those igneous or hydrothermal zircons, metamorphically modified zircon shows various secondary internal textures (e.g. Corfu et al., 2003). Although those modified textures are not necessary in order to know the formation mechanism, it has been relatively well understood as for two major types of the textures; one, recrystallization texture is the texture that had entirely or partly homogenized pristine texture. The other one, resorption-reprecipitation texture is the rounded bands (which also called “flow texture”) that developing around remaining pristine core. The latter is considered to be involved with metamorphic fluid and the similar one “convoluted texture”, which has irregular and discontinuous rounded bands, seems to have a similar formation mechanism (Bomparola et al., 2007).

Igneous and hydrothermal zircon rarely has secondary internal texture as compared with metamorphic zircon. However, a few recent studies described the multiple events on igneous and hydrothermal zircon and they discussed the geological



history based on the internal texture (da Silva et al., 2005; Kebede et al., 2007; Grant et al., 2009).

### ***Chemical features***

Zircon contains various trace elements.  $\text{Hf}^{4+}$ ,  $\text{U}^{4+}$  and  $\text{Th}^{4+}$  are incorporated in zircon structures by substituting  $\text{Zr}^{4+}$  ion and normally included in zircon for approximately 0.1 to 2.0 wt%.  $\text{Y}^{3+}$ ,  $\text{Sc}^{3+}$ , REEs and  $\text{P}^{5+}$  are replaced with a pair of  $\text{Zr}^{4+}$  and  $\text{Si}^{4+}$  through xenotime-type substitution (Finch and Hanchar, 2003; Hoskin and Schaltegger, 2003). Other trace elements such as  $\text{Nb}^{5+}$ ,  $\text{Ta}^{5+}$ ,  $\text{Fe}^{2+}$ ,  $\text{Mg}^{2+}$ ,  $\text{Al}^{3+}$ ,  $\text{Ca}^{2+}$  and  $\text{Ti}^{4+}$  are also included; however those impurities are present in extremely small quantity in zircon (Förster, 2006; Fu et al., 2008). In recent, zircon Ti thermometer was invented and applied on some natural zircons (Fu et al., 2008; Hiess et al., 2008; Claiborne et al., 2010).

Other than each impurity concentration, many zircon chemical studies have mentioned the total REE concentration, chondrite-normalized REE pattern (especially Ce/Ce\*), Zr/Hf ratio and Th/U ratio. Especially Th/U ratio has been commonly used to decide the growth environment whether igneous or metamorphic (e.g. Williams and Claesson, 1987; Rubatto, 2002, Koreshkova et al., 2009). The part of zircon which has Th/U ratio lower than 0.1 are regarded as metamorphic growth; the low Th/U ratio is caused by purification of the zircon crystal through recrystallization which associates with metamorphism. The Th/U ratio lowering is resulted from the different gaps of the ionic radii from  $\text{Zr}^{4+}$  between those cations ( $r_{\text{VIII}}^{\text{Zr}^{4+}}=0.84 \text{ \AA}$ ,  $r_{\text{VIII}}^{\text{U}^{4+}}=1.00 \text{ \AA}$ ,  $r_{\text{VIII}}^{\text{Th}^{4+}}=1.05 \text{ \AA}$ ; Finch and Hanchar, 2003).

## 2. Sample descriptions

I separated zircon grains from two rock samples of Cape Ashizuri Ring Complex, stage II quartz-syenite (II-QSy) and stage IV coarse biotite-granite (IV-CBG). The rock samples were collected in the localities which pointed in Fig. 6. Both rock samples are massive and nearly fresh, so I identified those samples as the lithofacies through comparing the results of microscopic observation (Fig. 7; as follows) to the data from Murakami et al. (1989).

II-QSy has granitic texture and medium grain size of 1.0 to 2.5 mm. It is mainly composed of quartz, alkali feldspar, plagioclase, biotite and hornblende. The alkali feldspar frequently shows string to rod perthite. The plagioclase is rather rare and it often shows rods to beads antiperthite, pericline twin and/or albite twin. Zircon, apatite, fluorite, thorite, chevkinite, allanite and Fe-Ti oxides are also included.

IV-CBG has granitic texture and coarse grain size of 3.0 to 7.0 mm including alkali feldspar megacrysts of about 1 cm long. It is mainly composed of quartz, alkali feldspar, plagioclase, biotite and hornblende. The alkali feldspar frequently shows strings perthite. The plagioclase often shows albite twin. Zircon, apatite, thorite and Fe-Ti oxides are also included.

Most of zircons are found in interstitial spaces among other minerals or included in biotite or hornblende; however fewer grains are included in other felsic minerals (Fig. 8). In these rocks, biotite and hornblende are commonly anhedral in shape and therefore they had crystallized at later stage of the magmatism. It is considered to be resulted from the anhydrous composition of A-type magma (e.g. Best and Christiansen, 2001).

Zircon grains were separated from these two rock samples through crushing, heavy liquid separation, magnetic separation and hand-picking (see Chapter 1 in detail). Separated zircon grains have typically about 300  $\mu\text{m}$  long, euhedral prismatic shape which surrounded by {100} and {101} planes and transparent reddish to brownish color.

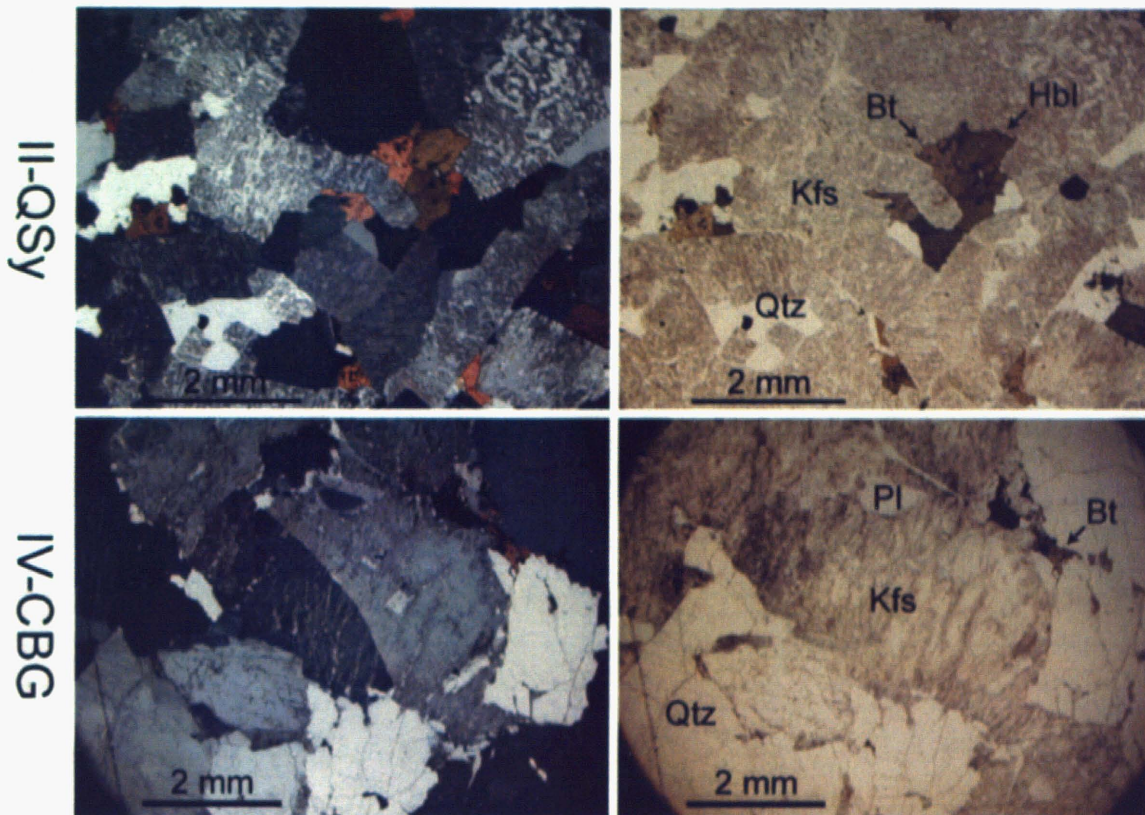


**Fig. 7.** Polarized optical microscope images of thin section of Cape Ashizuri Ring Complex. (a, b) II-QSy. (c, d) IV-CBG. (a, c) Crossed-polarized light. (b, d) Plane-polarized light. II-QSy, quartz-syenite (intrusion stage II); IV-CBG, coarse biotite-granite (intrusion stage IV); Qtz, quartz; Kfs, K-feldspar; Pl, plagioclase; Bt, biotite; Hbl, hornblende.

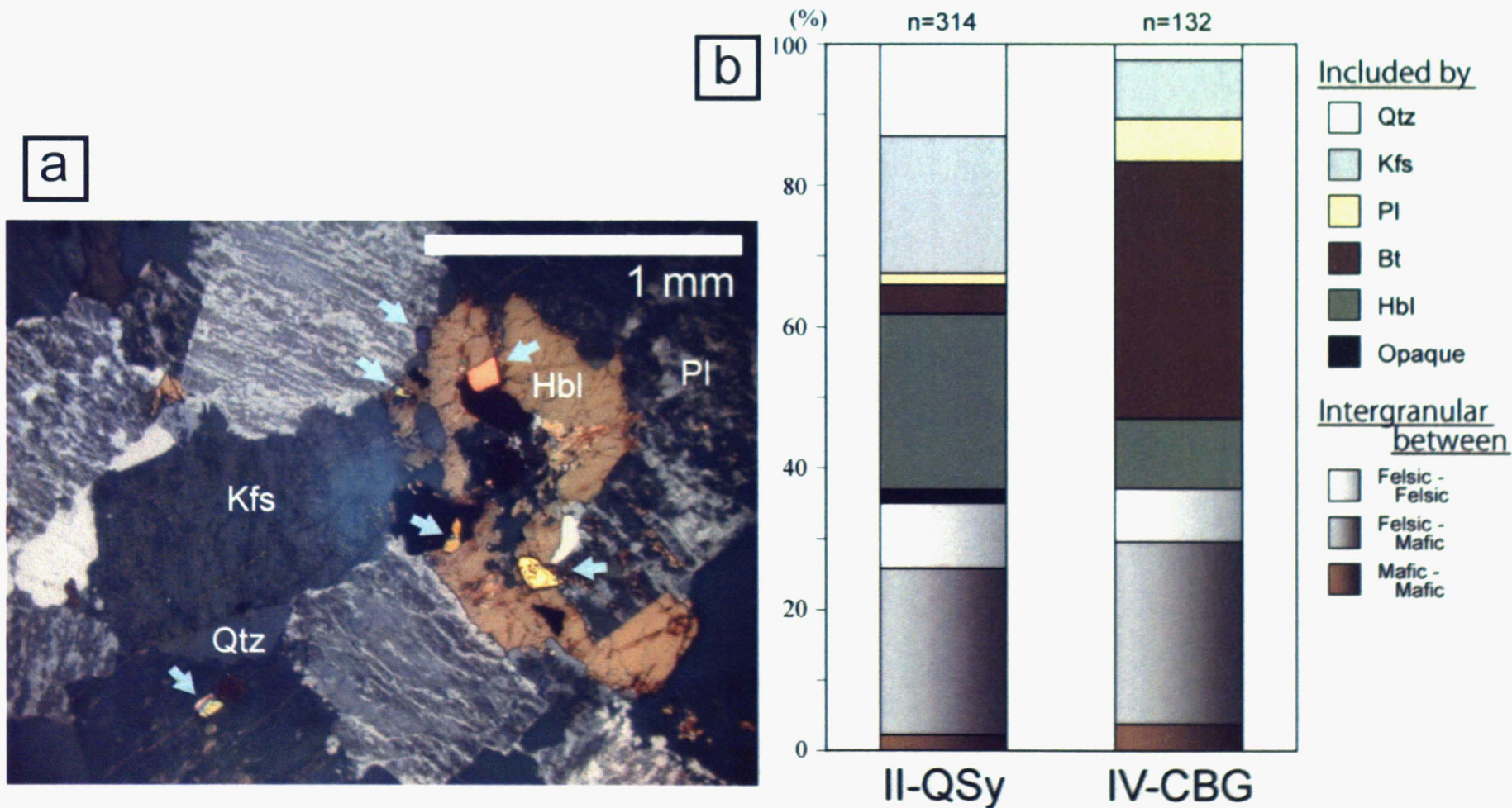


**Fig. 8.** (a) Polarized optical microscope image of thin section of Cape Ashizuri Ring Complex. Crossed-polarized light. Arrows indicate zircon. Qtz, quartz; Kfs, K-feldspar; Pl, plagioclase; Hbl, hornblende. (b) Statistic diagram of positional relations between zircon and the other minerals. included by, zircon is included by the mineral; intergranular between, zircon presents intergranular between the minerals; Qtz, quartz; Kfs, K-feldspar; Pl, plagioclase; Bt, biotite; Hbl, hornblende; Opaque, opaque minerals; Felsic-Felsic, felsic minerals (quartz, K-feldspar or plagioclase); Felsic-Mafic, felsic mineral and mafic mineral (biotite or hornblende); Mafic-Mafic, mafic minerals; II-QSy, zircon from quartz-syenite (intrusion stage II); IV-CBG, zircon from coarse biotite-granite (intrusion stage IV).

### 3. Analytical methods

Separated zircon grains were buried in epoxy resin, polished by 1  $\mu\text{m}$  diamond paste and then carbon-coated. I used this sample for SEM (JEOL JSM-5600) observation and Electron Probe Microanalyser (EPMA; JEOL JXA-8600) analysis. Thin sections of the two rock samples were also used for SEM and polarized microscope observations.

The SEM observation was carried out with 15 kV electron beam and BSE and CL images were corrected. All zircon internal textures which described on this study were definitely its own textures, not be artificial aspects made through sample preparation; that confirmed by BSE topological observation.

The chemical analyses using EPMA were carried out on quantitative point analysis and qualitative mapping analysis. Measured elements are  $\text{SiO}_2$ ,  $\text{ZrO}_2$ ,  $\text{HfO}_2$ ,  $\text{Y}_2\text{O}_3$ ,  $\text{UO}_2$ ,  $\text{ThO}_2$ ,  $\text{Ce}_2\text{O}_3$ ,  $\text{FeO}$  (including  $\text{Fe}_2\text{O}_3$ ),  $\text{CaO}$  and  $\text{P}_2\text{O}_5$  at quantitative point analysis and Si, Zr, Hf, Y, U and Th at qualitative mapping analysis. Other than that, for some samples Ce, Nd, P, Na, K, Ca, Ba, Fe, Mg, Mn, Al and Ti were also measured at the mapping analysis. The analytical conditions are 20 kV and 50 nA at quantitative point analysis and 15 kV and 500 nA at qualitative mapping analysis. Both analyses were carried out with 1  $\mu\text{m}$  probe diameter. At quantitative point analysis, the analytical times are 10 seconds for Si, Zr and Hf and 50 seconds for other trace elements. ZAF correction was applied for the quantitative results.

## 4. Results

### 4.1 Internal textures of zircon from Cape Ashizuri Ring Complex

Cape Ashizuri Ring Complex is doubtlessly considered to be an igneous complex, not to be a metamorphic suite. However most of zircon grains which included the ring complex have one or more kinds of “unusual” secondary internal texture (Fig. 9; the word “unusual” means the texture other than normal igneous zoning). I classified those unusual internal textures into three types; Resorption Disturbance texture (RD), Local Disturbance texture (LD) and Hafnon-like Disturbance texture (HD). Other than these textures, spongy cores and remained cores were also observed.

#### *Resorption Disturbance texture (RD)*

RD is rounded bands which dissolving igneous core (Figs. 9a-g). It develops from a past growth band toward core and no zircon sample shows two or more times of RD development in same grain. RD develops at only a part of past crystal surface, mainly at the corner, not at all-around crystal of the time. RD developments from present crystal surface or crack (it apparently shows a vein-like form) were rarely observed (Figs. 9e-g). While some convoluted zoning (Bomparola et al., 2007) were also rarely observed (Fig. 9d), I considered it to be complicated but closely related to RD in origin because both textures share similar banding feature and genetic interpretation.

#### *Local Disturbance texture (LD)*

LD is locally developing secondary texture (Figs. 9h-m). It is subdivided into two subtypes; one is locating at near core, LD1, and the other one is located at both core and rim, LD2. LD1 has a somewhat dendritic form and striped texture interiorly (Figs. 9h, i). By contrast, LD2 has fairly homogeneous interior and a round shape or a diffusing appearance toward rim from the generated area (Figs. 9i-m). Most of LD2 have lower BSE emission and higher CL emission than igneous texture of the same grain.

LD2 commonly generated from a characteristic inclusion; it has round shape and chiefly composed of anhedral minerals such as alkali feldspar, quartz and Na-rich plagioclase (Fig. 10). No relationship has found between the distribution region of LD2 and configuration of those minerals in the inclusion. The zircons are containing numerous euhedral apatite inclusions, however LD2 never shows the generation from the apatite inclusions. LD1 lacks such specific generation point but it seems to have developed from near the central of core, not from past crystal surface.

#### *Hafnon-like Disturbance texture (HD)*

HD has a penetrating distribution and an ameoboid irregular shape in cross-section (Figs. 9n-r; the name “Hafnon-like” originated from the after-mentioned chemical feature). It penetrated from present crystal surface to core deeply. HD has

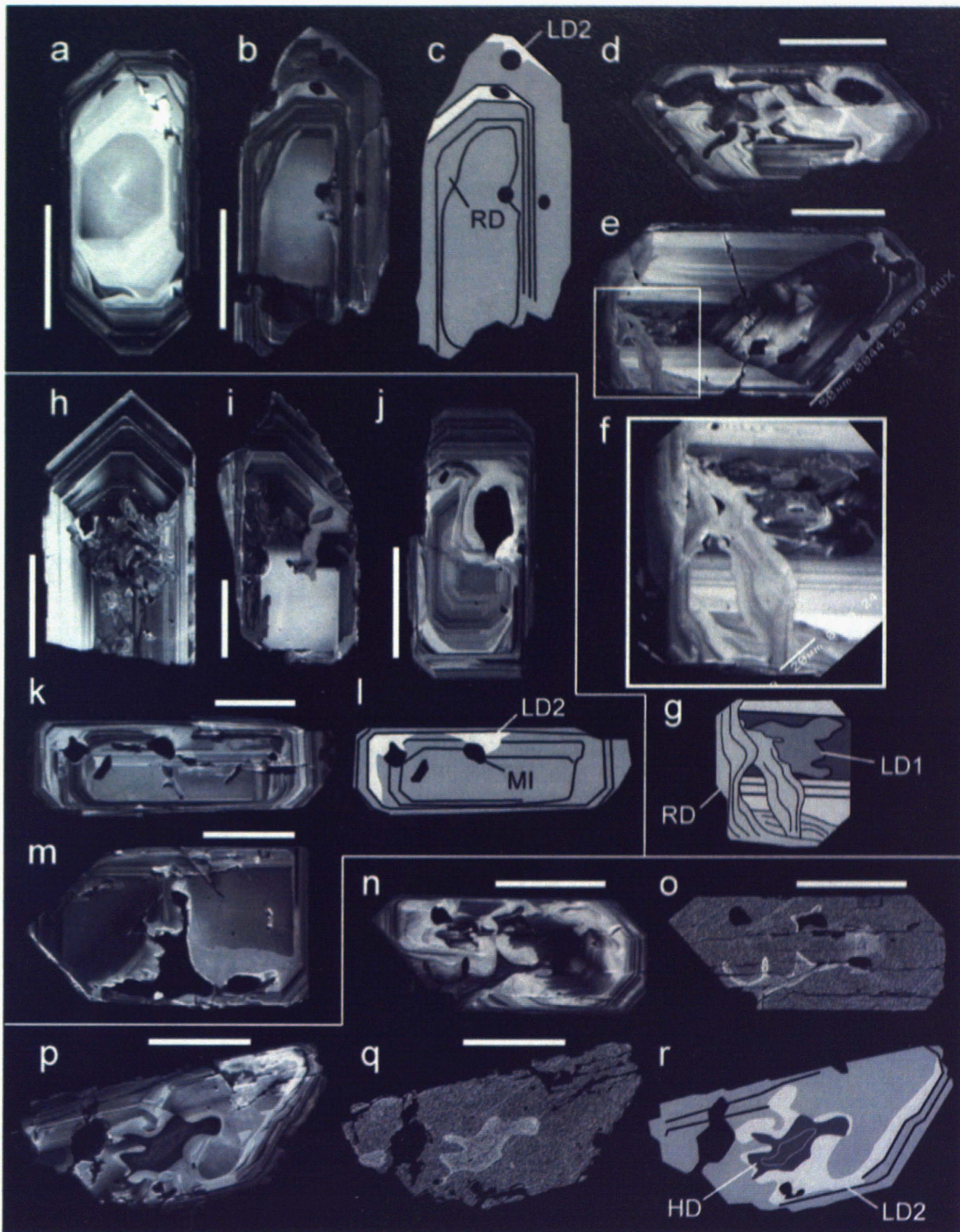


**Fig. 9.** Various internal textures of zircon from Cape Ashizuri Ring Complex. (a, b) RD, CL. (c, g, i, k, l, r) Model figures of (b), (f), (k) and (p), respectively. (d) RD like convoluted zoning, CL. (e, f) RD and "vein-like" RD, CL. The latter cuts across LD1 at core. The "vein-like" RD may have developed from fracture because other RD develops from physically broken edge and it seems likely to form another fractures. Furthermore, no RD shows penetrating development. (h, i) LD1, CL. (j-k, m) LD2, CL. The black areas are melt inclusion. See also Fig. 10. (n, p) HD, CL. (o, q) BSE images of (n) and (p), respectively. RD, resorption disturbance; LD1, local disturbance type-1; LD2, local disturbance type-2; MI, melt inclusion; HD, hafnon-like disturbance. Scale bars are 100  $\mu\text{m}$ .

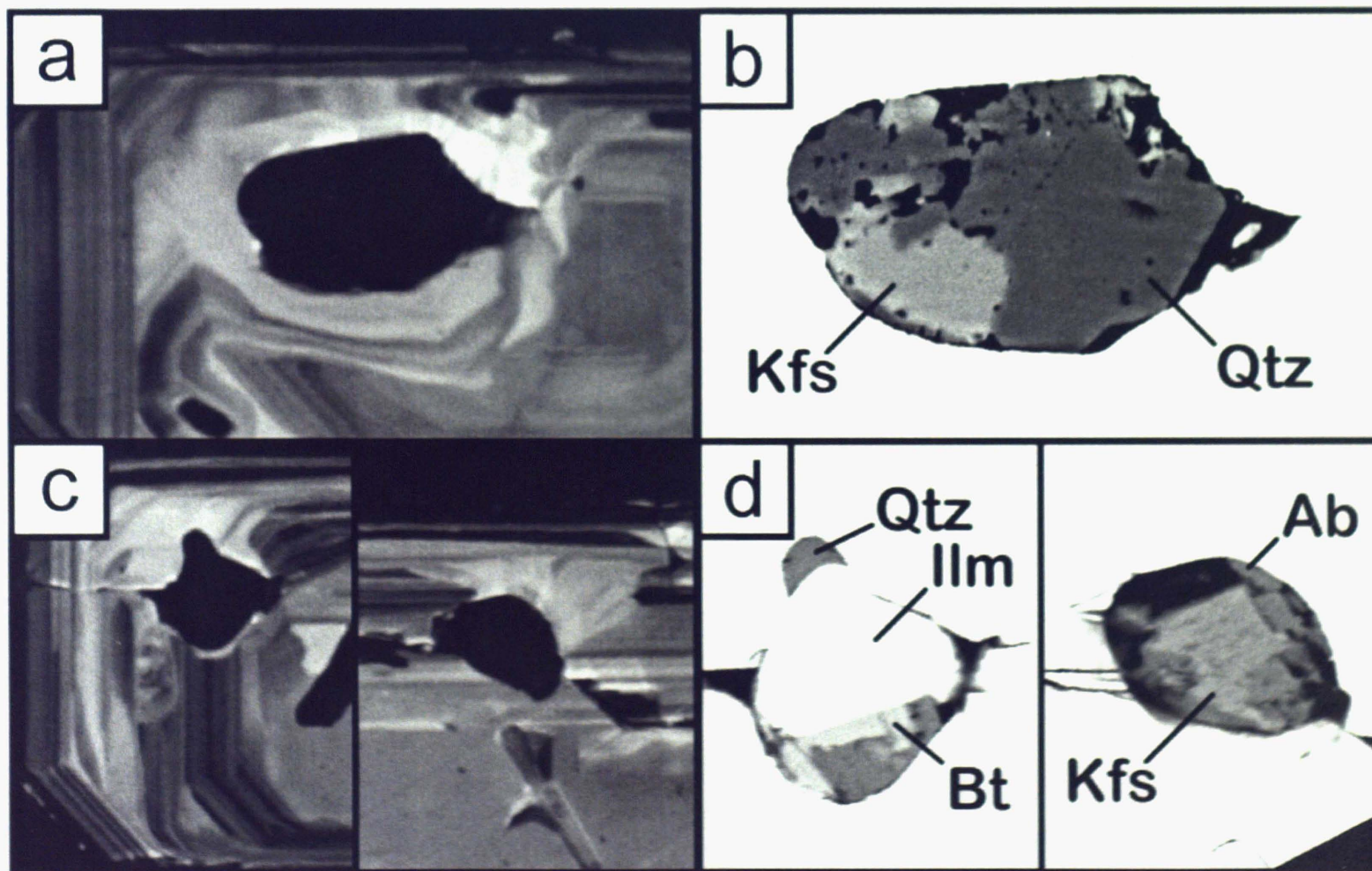


**Fig. 10.** Melt inclusions involved LD2. (a, b) Melt inclusion of Fig. 9j, CL and BSE. (c, d) Two melt inclusions of Fig. 9k, CL and BSE. The position of minerals has no influence on LD2. Qtz, quartz; Kfs, K-feldspar; Ab, albite; Bt, biotite; Ilm, ilmenite.



extremely higher BSE emission and lower CL emission than igneous texture; these features are pronounced at the outermost part of HD. HD shows flow texture interiorly and accompanied by a LD2-like CL-bright area at just outside. HD has only been found in IV-CBG zircons.

### ***Spongy core and remained core***

Zircons from Cape Ashizuri Ring Complex rarely have the core which shows spongy texture or dissolved shape (Fig. 11). The former is regarded as hydrothermal origin because of the numerous tiny inclusion (in other words, the core shows spongy texture) and very high BSE emission. Those hydrothermal cores have an original shape surrounded by planar surfaces, however a part of them are partially dissolved by RD at the boundary with igneous rim. One of the hydrothermal cores also shows LD1 and other case shows that LD2 develops in the spongy core from the adjacent round inclusion.

The latter, dissolved core is regarded as inherited core because of the all-around dissolved shape (the “inherited” also rewords as “recycled” or simply “remained”; e.g. Corfu et al., 2003; da Silva et al., 2005). The zircon grains which have these hydrothermal or remained cores are accompanied by radial fracture at the rim. The fracture is considered to be caused by different degree of metamictization between the core and rim (e.g. Lee and Tromp, 1995; Hoskin, 2005). In fact, both cores have high BSE emission that reflects high impurity concentrations including U and Th.

### ***Textural relationship among the secondary textures***

By SEM observations, following two relations among secondary textures were revealed; LD1 is cut by RD (Figs. 9e-g), LD2 distributes both inside and outside of RD (Figs. 9k, l). Depending on the relations, formation sequence of the secondary internal textures is strongly suggested as follows; (1) LD1, (2) RD and (3) LD2.

### ***Relationship between zircon internal texture set and surrounding minerals***

As noted above (see section 2), all rock-forming minerals of both rock samples include zircon. The presence of three secondary internal textures of zircon (LD1, RD and LD2) in each zircon-including mineral is listed in Fig. 12. Most of mineral phases contain zircon which has all three textures or at least LD2, however some mineral phases are not. No correlation was observed between adjacent mineral phase, and position or direction of zircon secondary internal texture.

The zircon included in plagioclase of II-QSy and quartz of IV-CBG is quite rare; I am considering that the former would be resulted from the small amount of plagioclase and the latter would result from the extremely low growth rate of quartz (also coarse-grained two feldspars of IV-CBG do not including a lot of zircon). I have not clearly recognized above secondary internal textures in these zircons so far, but a few zircons are included in the mineral phases (Fig. 8b). The alkali feldspars of II-QSy contain zircon which has only RD or LD1. Furthermore, these zircons have no or only thin igneous rim outside of the textures.

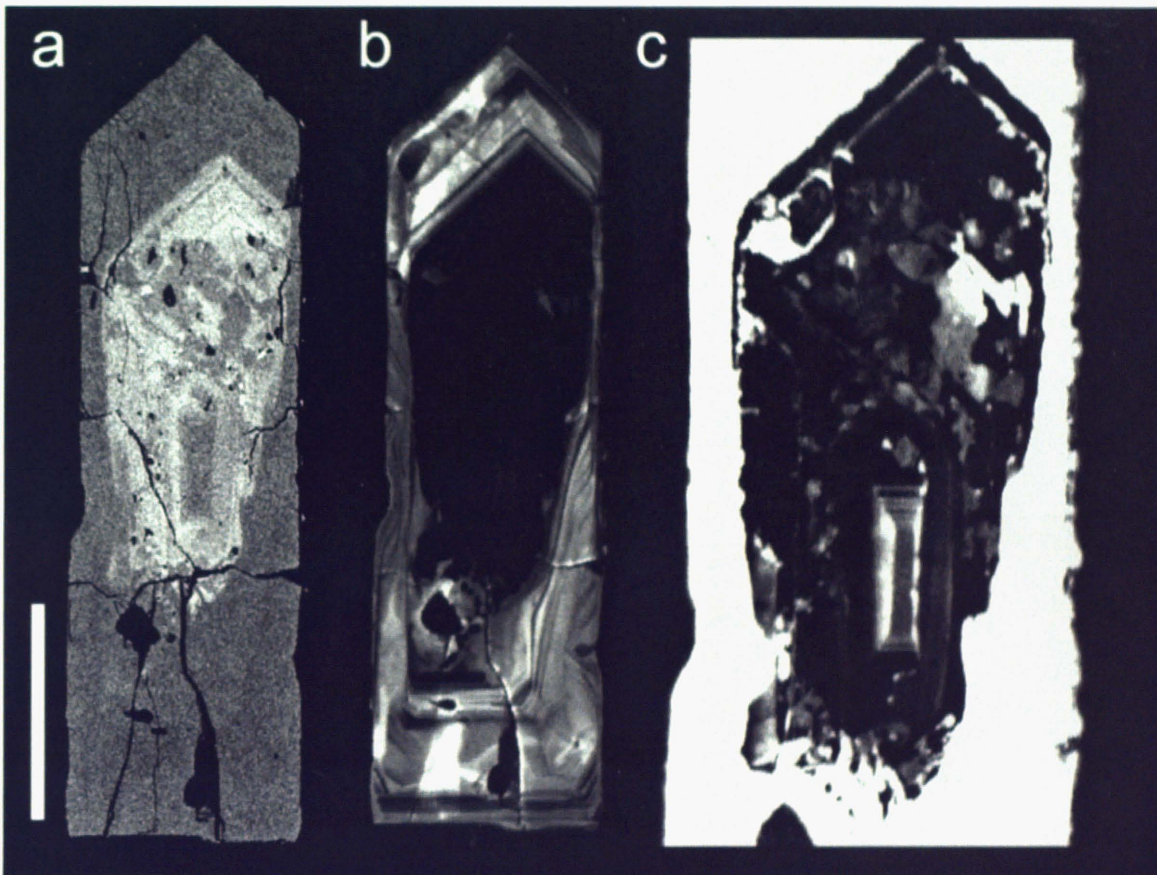


**Fig. 11.** Hydrothermal core of zircon from Cape Ashizuri Ring Complex. (a) Contrasting BSE emission of hydrothermal core and igneous rim, BSE. Radial fracture forms in rim. Scale bar is 100  $\mu\text{m}$ . (b) RD partly develops on the core, CL. (c) High magnification image of (b), CL. LD1 develops in the core.

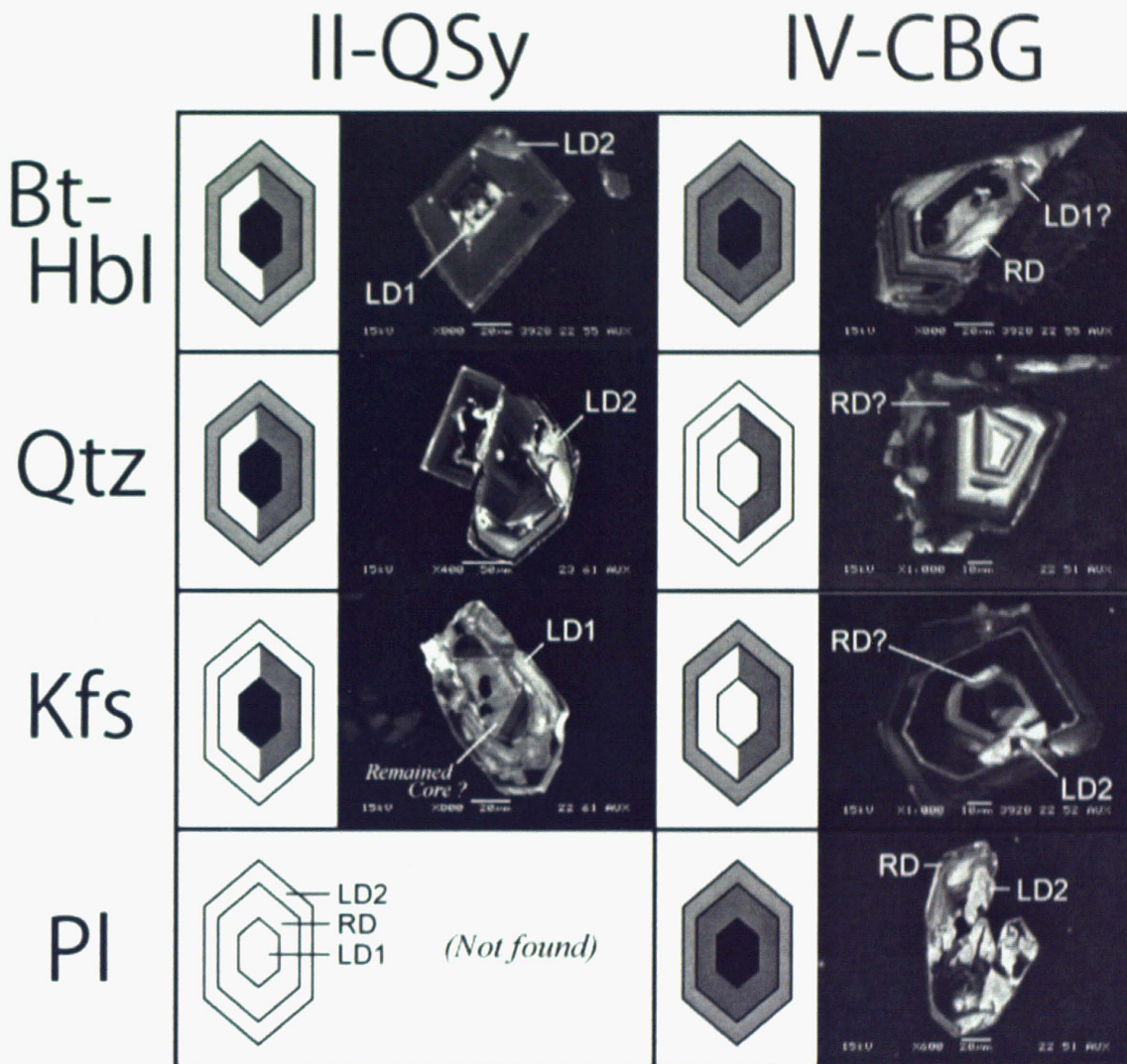


**Fig. 12.** Relationships between zircon-including mineral phase and secondary internal texture set of the zircon. Left column of each rock sample presents observed internal texture. Half-painted textures are not enough identified. Right column of each rock sample presents zircon which included in the mineral, CL. Zircon included in II-QSy plagioclase is quite rare but not strikingly absent. Zircons which exist between other minerals show all three secondary internal textures. The arrangement of mineral phases is roughly corresponds to crystallization sequence of each rock;  $Pl \approx Kfs \rightarrow Qtz \rightarrow Bt \approx Hbl$  (II-QSy),  $Pl \rightarrow Kfs \rightarrow Qtz \rightarrow Bt \approx Hbl$  (IV-CBG). Qtz, quartz; Kfs, K-feldspar; Pl, plagioclase; Bt, biotite; Hbl, hornblende; II-QSy, zircon from quartz-syenite (intrusion stage II); IV-CBG, zircon from coarse biotite-granite (intrusion stage

## 4.2 Chemical features of each internal texture – quantitative point analysis

While I measured 10 oxides on the EPMA quantitative point analysis as noted above, this section presents 4 oxides ( $\text{HfO}_2$ ,  $\text{Y}_2\text{O}_3$ ,  $\text{UO}_2$  and  $\text{ThO}_2$ ) which have notably distinction among each internal texture (Fig. 13). Selected results including all 10 oxides presented at Table 1.

### *Igneous texture*

Zircons from Cape Ashizuri Ring Complex have some compositional difference between the core and rim. On the  $\text{HfO}_2$  content, IV-CBG zircons is higher than II-QSy zircons and both rims are somewhat higher than each core (approximately 0.6 to 1.2 wt% in II-QSy zircons core, 0.9 to 1.3 wt% in II-QSy zircons rim, 0.9 to 1.2 wt% in IV-CBG zircons core and 1.3 to 1.5 wt% in IV-CBG zircons rim).  $\text{UO}_2$  contents are range from 0.02 to 0.62 wt%, the content in rim tends to be higher than that in core on IV-CBG zircons.  $\text{Y}_2\text{O}_3$  and  $\text{ThO}_2$  contents are range from 0.05 to 1.19 wt% and range from 0.01 to 0.65 wt%, respectively. There is no significant difference on these oxides content between core and rim. Th/U ratios are range from 0.1 to 1.2.

### *RD*

Although the  $\text{HfO}_2$  contents of RD show a wide distribution (0.96 to 2.03 wt%), it totally tends to be higher than those of igneous texture. Conversely, the  $\text{Y}_2\text{O}_3$ ,  $\text{UO}_2$  and  $\text{ThO}_2$  contents are mainly lower than those of igneous texture. Th/U ratios are range from 0.1 to 1.0.

### *LD*

LD has totally lower  $\text{Y}_2\text{O}_3$  and  $\text{ThO}_2$  contents and slightly higher  $\text{HfO}_2$  contents than igneous texture. Th/U ratios are lower than those of igneous texture and distribute wide range (0.02 to 1.0).  $\text{UO}_2$  contents of LD1 are higher than those of LD2, therefore LD1 have lower Th/U ratios.

### *HD*

HD is characterized by the extremely high  $\text{HfO}_2$  content which is range from 2.04 to 2.60 wt%, so the texture can be seen as zircon solid solution which is rich in hafnon ( $\text{HfSiO}_4$ ) component.  $\text{Y}_2\text{O}_3$  and  $\text{ThO}_2$  contents of HD are clearly lower than those of igneous texture (0.01 to 0.06 wt% and <0.01 wt%, respectively), on another front the  $\text{UO}_2$  contents showing high value as much as rim (0.11 to 0.28 wt%). As a result, all values of Th/U ratio fall below 0.1.

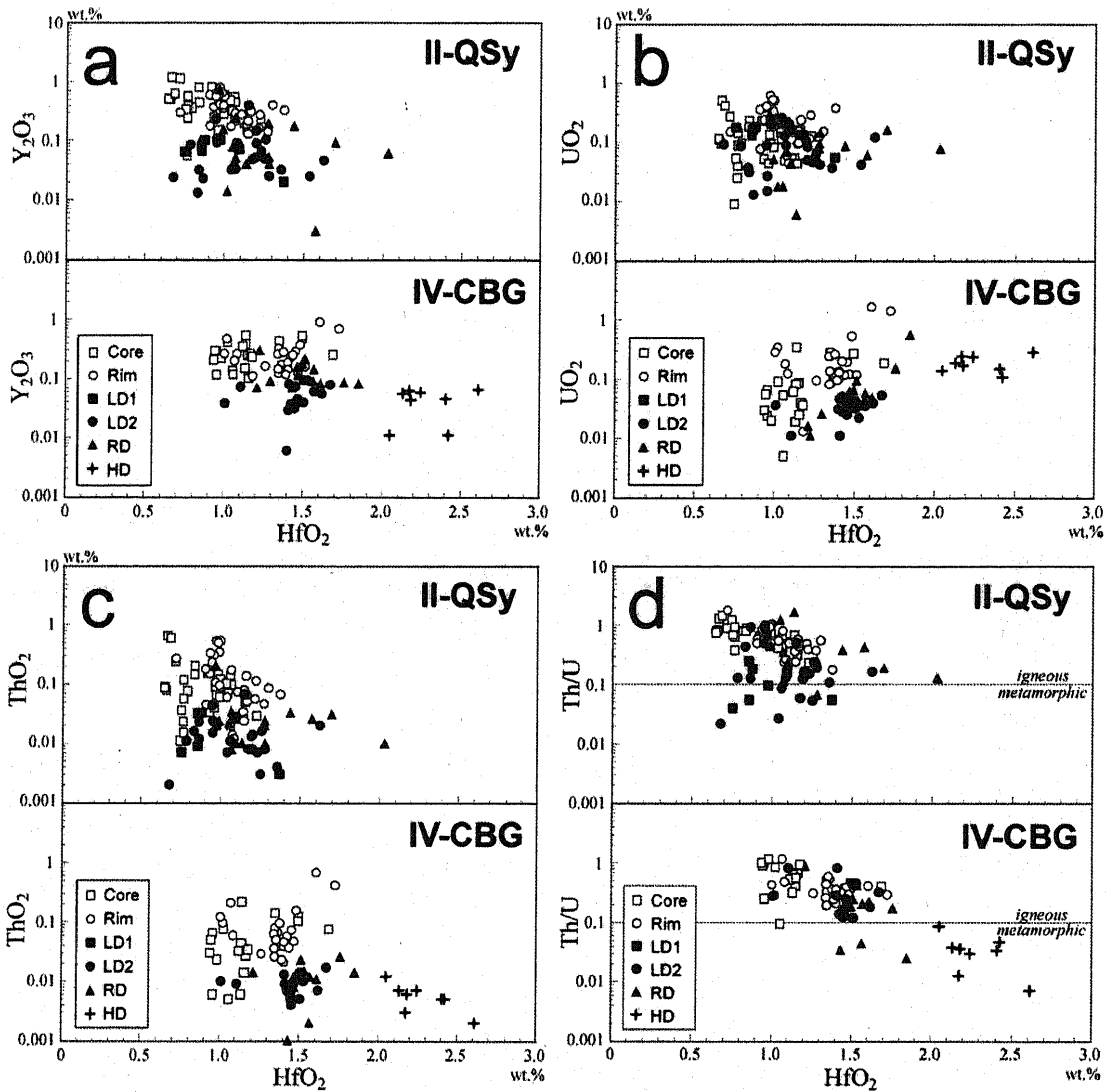


**Fig. 13.** Relationships between  $HfO_2$  and (a)  $Y_2O_3$ , (b)  $UO_2$ , (c)  $ThO_2$  and (d) Th/U of zircon from Cape Ashizuri Ring Complex. II-QSy, zircon from quartz-syenite (intrusion stage II); IV-CBG, zircon from coarse biotite-granite (intrusion stage IV).

**Table 1.** Representative chemical data of zircon from Cape Ashizuri Ring Complex.

Rock Sample II-QS																
Texture Type	Core	Core	Core	Rim	Rim	Rim	Rim	LD1	LD1	LD2	LD2	LD2	LD2	RD	RD	RD
Analysis No.	1005C1	1101C1	1110C1	1004R1	1004R2	1104R1	1110R2	1007I2	1106I5	1104I2	1104I4	1105I1	1106I1	1004O2	1009O2	1104O1
(wt%)																
SiO <sub>2</sub>	33.86	33.40	33.41	34.21	33.89	34.04	34.23	34.55	34.63	34.76	33.93	33.57	34.16	34.94	34.53	33.69
ZrO <sub>2</sub>	66.40	66.38	64.90	65.51	64.29	65.05	64.65	66.30	65.25	64.39	65.64	64.81	66.37	64.83	65.34	65.33
HfO <sub>2</sub>	0.80	1.15	1.07	1.15	1.30	0.94	0.91	0.87	0.88	0.95	1.18	1.15	0.84	1.29	1.00	1.58
Y <sub>2</sub> O <sub>3</sub>	0.37	0.18	0.45	0.14	0.40	0.62	0.60	0.07	0.10	0.23	0.05	0.40	0.01	0.05	0.16	n.d.
UO <sub>2</sub>	0.10	0.05	0.22	0.10	0.16	0.40	0.37	0.17	0.18	0.09	0.14	0.13	0.04	0.10	0.05	0.06
ThO <sub>2</sub>	0.08	0.03	0.10	0.03	0.09	0.34	0.18	0.01	0.03	0.04	0.01	0.07	0.02	0.03	0.02	0.03
Ce <sub>2</sub> O <sub>3</sub>	0.02	0.01	0.01	0.01	0.02	0.03	0.02	0.01	0.02	0.03	0.02	0.02	0.02	0.02	0.02	0.02
FeO	n.d.	n.d.	0.01	n.d.	n.d.	n.d.	0.01	0.01	0.01	n.d.	0.01	0.01	n.d.	0.01	0.01	0.01
CaO	n.d.	0.01	n.d.	0.01	0.03	n.d.	0.02	0.03	0.01	n.d.	0.01	0.01	n.d.	n.d.	0.02	0.01
P <sub>2</sub> O <sub>5</sub>	0.04	0.04	0.06	0.06	0.07	0.09	0.10	0.07	0.06	0.05	0.03	0.06	0.03	0.04	0.03	0.04
Total	101.66	101.23	100.23	101.22	100.24	101.50	101.07	102.08	101.17	100.55	101.01	100.23	101.49	101.31	101.18	100.77
Th/U ratio	0.798	0.680	0.432	0.357	0.550	0.849	0.492	0.054	0.182	0.493	0.058	0.502	0.431	0.249	0.460	0.425

Rock Sample IV-CBG																
Texture Type	Core	Core	Core	Rim	Rim	Rim	Rim	Rim	LD2	LD2	LD2	RD	RD	RD	HD	HD
Analysis No.	1308C2	1312C2	1316C1	1306R2	1312R2	1313R1	1316R1	1316R2	1303I1	1310I2	1312I1	1304O1	1304O2	1313O2	1316A3	1316A4
(wt%)																
SiO <sub>2</sub>	33.59	34.48	33.73	34.09	33.88	33.48	34.10	34.41	33.83	33.95	33.68	33.40	34.07	33.81	33.49	33.64
ZrO <sub>2</sub>	64.89	65.01	64.26	63.62	65.28	62.94	63.52	63.22	64.26	64.42	64.75	63.67	63.34	64.01	63.15	63.33
HfO <sub>2</sub>	0.94	1.19	1.15	1.34	1.36	1.46	1.39	1.38	1.46	1.00	1.41	1.59	1.52	1.49	2.60	2.16
Y <sub>2</sub> O <sub>3</sub>	0.29	0.23	0.10	0.32	0.12	0.36	0.14	0.12	0.05	0.04	0.08	0.08	0.09	0.18	0.06	0.06
UO <sub>2</sub>	0.06	0.04	0.03	0.24	0.14	0.52	0.13	0.10	0.04	0.04	0.01	0.05	0.04	0.07	0.28	0.24
ThO <sub>2</sub>	0.05	0.03	0.01	0.08	0.03	0.15	0.05	0.02	0.01	0.01	0.01	0.01	0.02	0.01	n.d.	n.d.
Ce <sub>2</sub> O <sub>3</sub>	0.04	0.02	0.04	0.03	0.03	0.02	0.04	0.04	0.02	0.03	0.02	0.03	0.02	0.02	0.04	0.03
FeO	n.d.	0.01	n.d.	0.01	0.01	n.d.	n.d.	n.d.	0.01	0.01	0.01	0.01	n.d.	n.d.	n.d.	0.01
CaO	0.03	n.d.	0.02	n.d.	0.01	0.01	0.01	0.02	0.01	0.01	n.d.	n.d.	0.02	n.d.	n.d.	0.01
P <sub>2</sub> O <sub>5</sub>	0.07	0.08	0.05	0.18	0.08	0.11	0.07	0.08	0.05	0.04	0.08	0.06	0.10	0.15	0.04	0.06
Total	99.96	101.08	99.39	99.91	100.94	99.05	99.44	99.38	99.72	99.56	100.04	98.90	99.21	99.73	99.67	99.54
Th/U ratio	0.906	0.942	0.558	0.327	0.192	0.292	0.355	0.241	0.249	0.277	0.816	0.224	0.415	0.184	0.007	0.012

Th/U is atom ratio. n.d., not detected.

### **4.3 Chemical features of each internal texture – qualitative mapping analysis**

While I measured 6 elements and partly 12 extra elements on the EPMA qualitative mapping analysis as noted above, this section presents particular elements which show a clear difference between unusual secondary texture and igneous texture (Fig. 14). The analyzed samples have LD1, LD2 and HD.

#### ***LD***

Both of LD1 and LD2 have lower Y and Th contents and slightly higher Hf contents than adjacent igneous texture. Whereas U contents of LD2 are clearly lower than igneous texture, LD1 has U content similar to that of adjacent igneous texture. It indicates that LD1 has lower Th/U ratio than LD2. One example of LD2 shows a distinguishing chemical behavior; some trace elements such as Y and U distribute in high concentration at the region just outside of LD2 despite the region of LD2 shows low concentration of the elements.

#### ***HD***

HD shows the obviously high concentration of Hf. Moreover, HD and the LD2-like texture which accompanying HD barely show different U and Th concentrations from adjacent igneous texture.

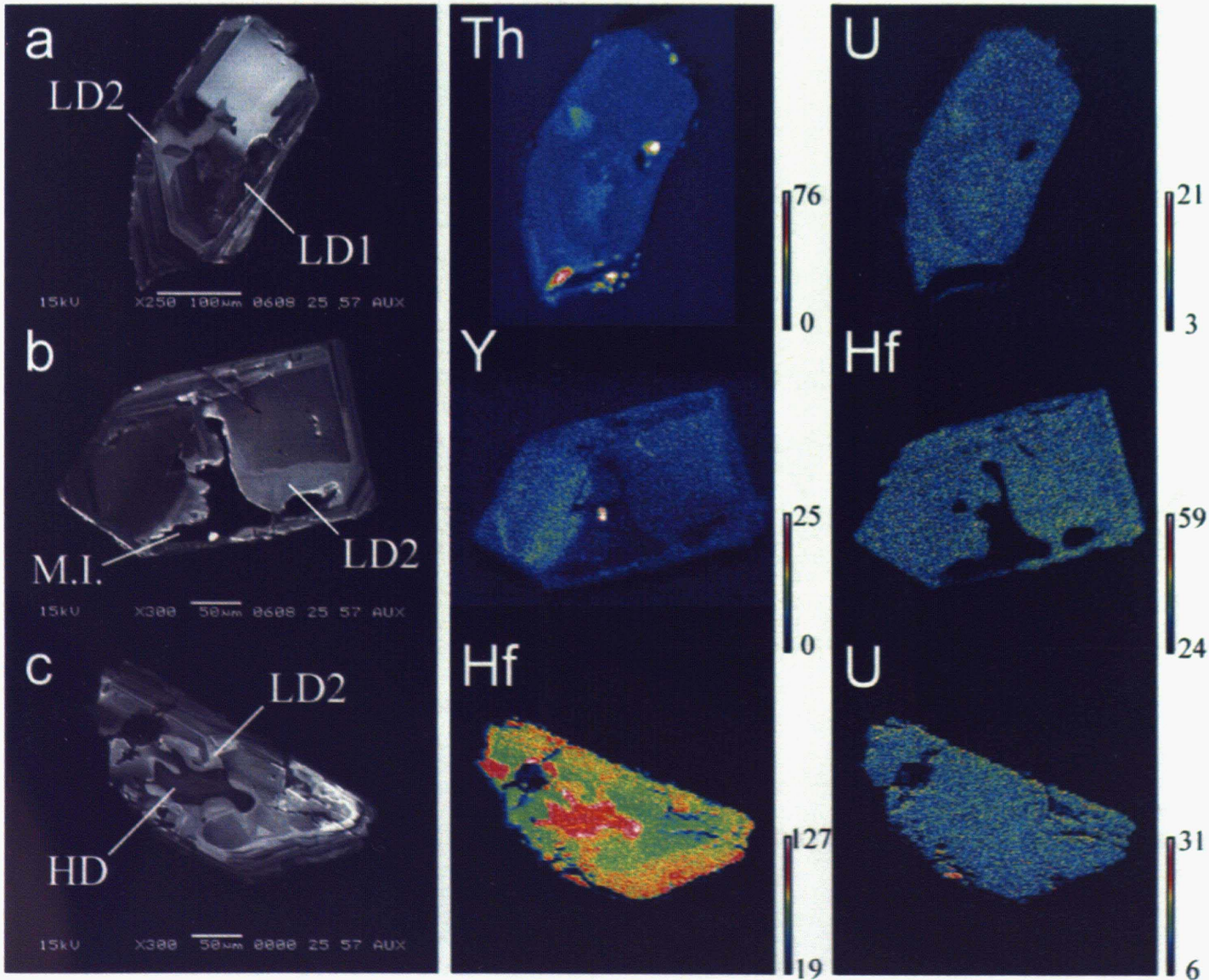


**Fig. 14.** Various internal textures and corresponding elemental behavior of zircon from Cape Ashizuri Ring Complex. Numbers are indication of the X-ray intensity. The CL image and Y distribution of (b) shows recrystallization front, which is located at outside of the recrystallized area and characterized as high concentrations of the elements purged by the recrystallization (Fig. 11b of Hoskin and Schaltegger, 2003). Left column, CL; Others, X-ray mapping images.



## 5. Discussion

### 5.1 Formation mechanism of the secondary internal textures

Various unusual internal textures of zircon from Cape Ashizuri Ring Complex seem to have been formed during the magmatic evolution; because most of those textures are consistently showing the development within the crystal, not from the present crystal surface, so most of those textures must not have been formed by post-magmatic alteration. Therefore, the unusual internal textures of zircon must contain valuable information on the magmatic histories, which correspond to the transition of their growth environments.

The formation mechanism of zircon secondary internal textures is still less well understood; however, there is rough classification of the secondary internal textures and some knowledge about the corresponding formation mechanism (Corfu et al., 2003; Grant et al., 2009). So, I have compared the zircon internal textures which found on this study with previous reports.

#### ***RD***

The textural features of RD are quite similar to resorption-reprecipitation texture which mainly seen in metamorphic zircon, especially the rounded banding pattern and the distribution along grain surface of the time (e.g. Vavra et al., 1996; Nutman et al., 2002). The resorption-reprecipitation texture is commonly considered to reflect the Zr-undersaturated environment and following overgrowth (Corfu et al., 2003). The fact that RD develops at a part of the grain surface must indicate the Zr-undersaturation was mildly or the undersaturated melt contacted at narrow region of zircon surface.

Although convoluted zoning may be interpreted by infiltration of metamorphic fluid (Bomparola et al., 2007), no evidence which indicates metamorphism has been found in Cape Ashizuri Ring Complex. Moreover, most of RD have Th/U ratio above 0.1 which considered as an index of metamorphic growth (e.g. Williams and Claesson, 1987; Rubatto, 2002).

#### ***LD2***

LD2 resembles local recrystallization texture of igneous or metamorphic zircon closely in the developing form and chemical features (e.g. Figs. 10a, 11b of Hoskin and Schaltegger, 2003; Fig. 7 of Tomaschek et al., 2003; da Silva et al, 2005). The local recrystallization texture of igneous zircon is explained by involvement of late-stage magmatic fluid (Corfu et al., 2003; Nemchin and Pidgeon, 1997) or solid-state recrystallization (Hoskin and Black, 2000; Hoskin and Schaltegger, 2003).

LD2 seems to be closely related to the inclusion with multiple mineral phases (Fig. 10). I think that this inclusion must correspond to slowly-cooled alkali granitic melt inclusion; because of the round shape as an inclusion, anhedral-shape-dominant mineral aggregation, grain size and mineral composition. The minerals were not

crystallized on the time of LD2 had formed because the mineral configuration is not related to LD2 distribution. So, LD2 development must have been closely related to the melt inclusion. Not to say, the melt contains some fluid phases, therefore it is likely that LD2 is fluid-related recrystallization texture. It seems that the distinction between internal pressure of included melt and pressure of outside melt has increased as magma uplifting, so the outward development which are seen in some LD2 may be caused by the pressure distinction and resulting volatile infiltration.

However LD2 on this study shows recrystallization front as purges of Y and U which reported on the description of solid-recrystallization (Fig. 14b; Hoskin and Black, 2000). The true formation mechanism of LD2 is still unclear, but it must be local recrystallization texture. The mild decreasing of Th/U ratio would be explained by the limited amount of included melt and resulting incomplete redistributions of those impurities.

### ***LD1***

LD1 is also quite similar to local recrystallization texture which reported by Tomaschek et al. (2003) in the textural and chemical feature. LD1 has not obvious generated area such as melt inclusion of LD2, and in addition it never developed from the crystal surface, hence LD1 would not have been caused by fluid-induced recrystallization. Solid-state recrystallization, which is another mechanism of local recrystallization, is considered to result from resolution of unstable crystal state with decreasing temperature (Hoskin and Schaltegger, 2003).

### ***HD***

HD has many unique features. An involvement of fluid phase is deduced from the accompanying LD2-like texture (as fluid-induced recrystallization texture), development from present surface and only high Hf concentration unlike other impurities. The last two features are also seen in recrystallized texture, as with the low Th/U ratio and the particularly high Hf concentration at outermost part (it can be regarded as impurity purging like recrystallization front). However, LD2-like (recrystallization?) texture around HD and internal flow texture are negative about the assumption. Flow texture is characteristic feature of resorption-reprecipitation texture, but the penetrating development from present surface to core deeply is negative about the mechanism.

To reveal HD formation mechanism, the only high Hf concentration is particularly peculiar feature; because each impurity content in zircon is considered to largely depend on the deference of ionic radii from  $Zr^{4+}$  (0.84Å), so  $Hf^{4+}$  (0.83Å) has the weakest character as zircon impurity component (Finch and Hanchar, 2003; Hoskin and Schaltegger, 2003). For the same reason Zr and Hf always show quite similar behavior and therefore Zr/Hf ratio of both zircon and melt not depend on whether it is igneous or metamorphic origin but determined by the melt composition such as alkalinity (Brooks, 1969; Linnen and Keppler, 2002). However, some of late-magmatic fluids seem to have high Hf content and low Zr/Hf ratio because hafnon has commonly

found in pegmatitic environment. This indicates that HD may have been formed by Hf-enriched post- or late-magmatic fluid phase.

### ***Spongy core and remained core***

Spongy texture with high BSE emission is main characteristic of hydrothermal zircon (e.g. Hoskin, 2005; Pelleter et al., 2007; Hoshino and Ishihara, 2007). The spongy cores observed on this study also retain nearly original morphology (without RD), so it must be regarded as hydrothermal core which igneously overgrown as the rim.

Remained core is commonly regarded as residue of source rock which had partially melted and generated magma that corresponded to growth environment of the zircon rim. This interpretation is applied when the remained core is found in igneous zircon (da Silva et al., 2005; Grant et al., 2009), such report is relatively rare than in metamorphic zircon.

The remained core on this study would not have same implication with above hydrothermal core; it has all-around dissolved shape, not as same with the hydrothermal core, so the remained core had doubtlessly been constituent of the source rock of Cape Ashizuri Ring Complex but the hydrothermal core would have been formed in the subsequently generated magma (strictly the latest fluid phase). It also indicated that a hydrothermal fluid phase would have existed before RD was formed.

## **5.2 Growing sequence of the internal textures**

Based on the forming sequence of both secondary internal textures and primary igneous zoning, following six growth stages are supposed on the zircons from Cape Ashizuri Ring Complex (Figs. 15, 16).

**Stage I:** Igneous and hydrothermal core had crystallized. Some of the igneous core was overgrown from previously existed (remained) zircon core.

**Stage II:** LD1 had been formed in igneous/hydrothermal core. It would be solid-state recrystallization texture and caused by temperature decreasing.

**Stage III:** RD had been formed at partially around core. It would be caused by Zr-undersaturation and following overgrowth.

**Stage IV:** Igneous rim had grown. The chemical composition, temperature and/or pressure of surrounding melt would be different from that when core had grown because  $\text{HfO}_2$  and  $\text{UO}_2$  concentrations are clearly different between core and rim. Some of melt inclusions are cutting oscillatory zoning of core, so the melt inclusions may have trapped at embayed zircon surface during this stage. The shape of melt inclusion such as Fig. 9m is well explaining the melt trapping mechanism as such hollow-filling by melt and sealing by subsequent igneous zircon growth. However, a few melt inclusions which apparently have no correlation with dissolving event (RD) are also observed.

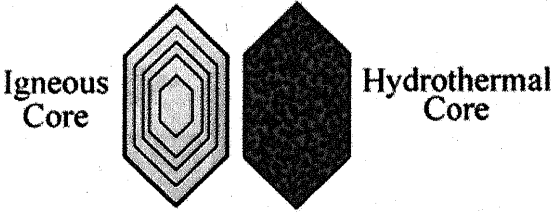


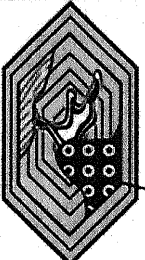
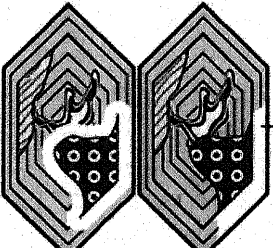
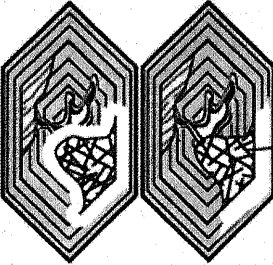
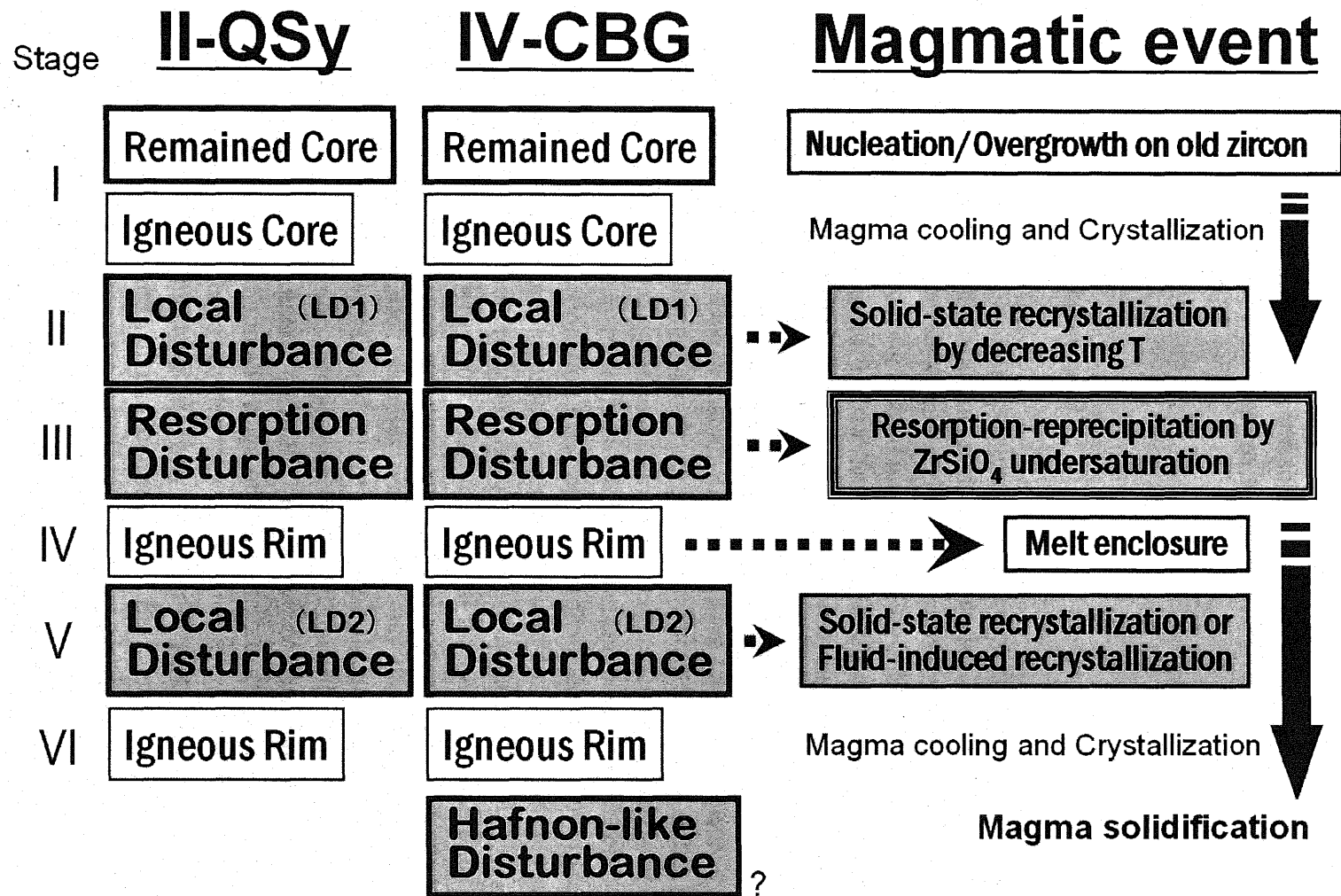
Growth Stage	Model Figure
1	 <p>Igneous Core      Hydrothermal Core</p>
2	 <p>Forming LD1</p>
3	 <p>Forming RD (Resorption-Recipitation)      Resorption</p>
4	 <p>Magmatic Overgrowth      Entrapped Melt</p>
5	 <p>Forming LD2 around Melt Inclusions</p>
6	 <p>Magmatic Overgrowth      Slow Cooling of Melt Inclusions</p>

Fig. 15. Model figure of development of internal textures of zircon from Cape Ashizuri Ring Complex. See text in detail.



**Fig. 16.** Relations between zircon internal textures and corresponding magmatic event in Cape Ashizuri Ring Complex. The leftmost column represents six growth stages of zircon (see also Fig. 15). Gray squares represent zircon secondary internal textures and corresponding environmental changes. II-QSy, zircon from quartz-syenite (intrusion stage II); IV-CBG, zircon from coarse biotite-granite (intrusion stage IV).

**Stage V:** LD2 had formed around melt inclusions. It would be local recrystallization texture which related to the melt inclusions. The two development types of LD2, all-around development and outward diffusion both from melt inclusion would be formed at same stage.

**Stage VI:** Igneous outermost rim had grown. This growth band is not being reprinted by LD2. Slow-cooling and solidification of melt inclusions would have carried out at this stage because LD2 seems to be formed when the melt inclusions were not solidified.

### 5.3 Zr-undersaturation event

I think the most important internal texture of the zircon in consideration of the magmatic evolution of Cape Ashizuri Ring Complex is RD. It clearly shows a past disequilibrium situation between the zircon and surrounding environment. Although of course it did not arise during normal magma cooling and associated fractionation, RD is found in both zircons of II-QSy and IV-CBG. So this unusual texture might be suggesting the distinctive event of which elucidates the uncommon occurrence of this A-type suite.

RD and the adjacent igneous textures strongly indicate two things about the undersaturation event. One is that all RD would have formed at only one time, depends on absence of the multiple-stage development evidence. The other is that RD must have been accompanied by a significant change of chemical composition, temperature and/or pressure of surrounding melt; it is based on the compositional difference that is less consisted with the fractionation trend between igneous core and rim of the zircons (Fig. 17). However, such one significant magmatic event has been reported neither on any other minerals nor whole rock analysis so far (cf. Murakami et al., 1989).

The reasons why other minerals without zircon do not have the record would include the crystallization sequence and mineral composition of Cape Ashizuri Ring Complex. Both two rock samples which used on this study have anhedral (lately crystallized) mafic minerals and minor amount of plagioclase; it is generally explained by anhydrous and alkalic composition of A-type magma. Therefore, calcic plagioclase and typical hydrous mafic minerals such as biotite and hornblende must not have crystallized on early magmatic stage of this A-type suite, so zircon seems to be one of the few minerals that had recorded the early magmatic environment.

Remaining problems are why zircon-coexisted other minerals such as alkali feldspar or low amounts of plagioclase do not have record of the Zr-undersaturation event and what was the event. Alkali feldspars and plagioclases of my two rock samples do not show evidence of which indicates magma mixing or other significant nonequilibrium condition, it is consistent with previous studies. I will try to estimate the magmatic event and associated deletion of the record in crystallized minerals without zircon by the following discussion based on three presumable cases (Fig. 18).

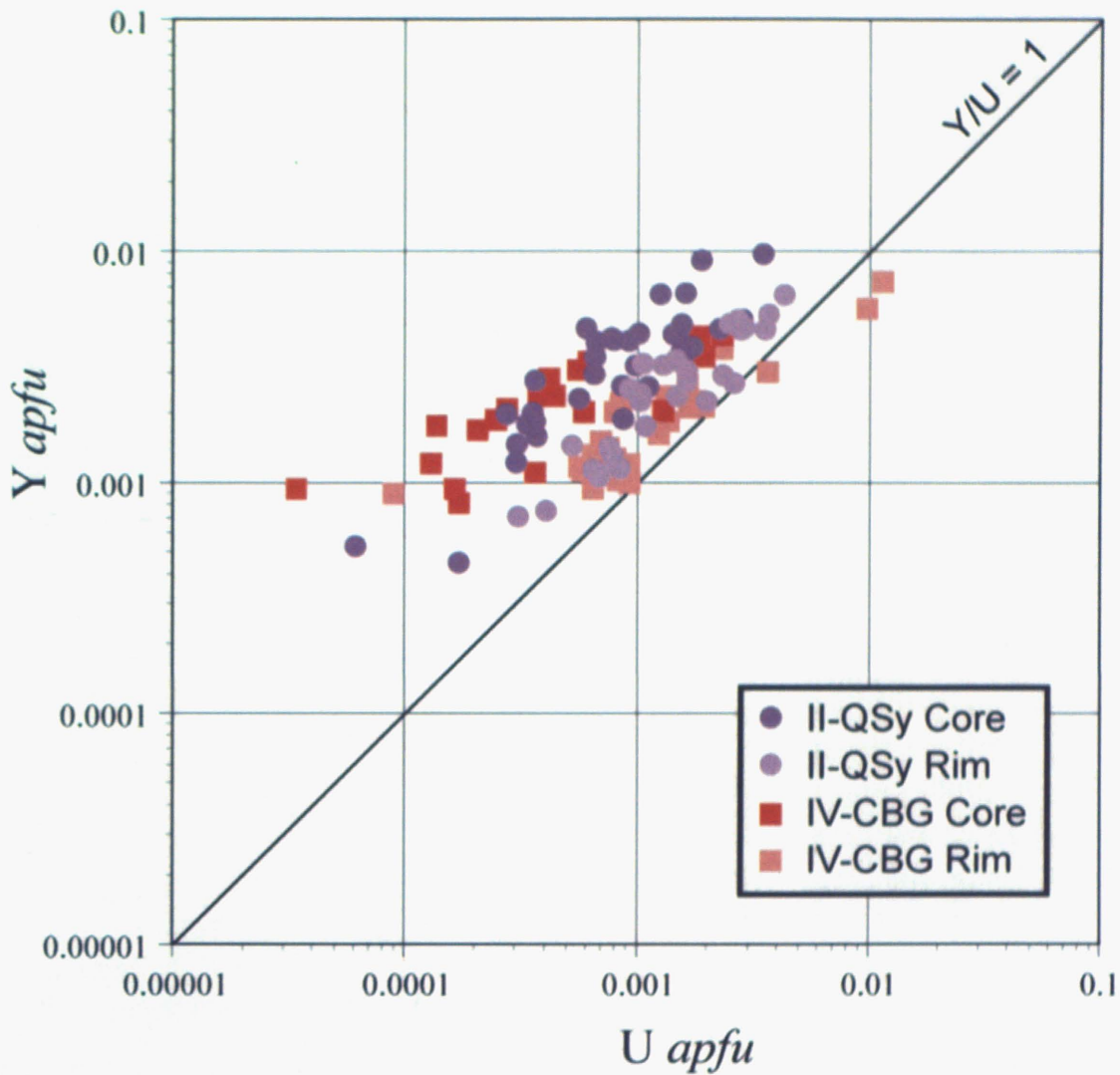


**Fig. 17.** Relationship between U and Y of zircon from Cape Ashizuri Ring Complex. Datas are same with Fig. 13 but recalculated for atom per formula unit (apfu) on the basis of 4 oxygen atoms. Fractional trend within same texture is upward from left to right nearly parallel with the line  $Y/U=1$ , it is consistent with the transition of partition coefficients of these elements as temperature decreases (see also Fig. 19). II-QSy, zircon from quartz-syenite (intrusion stage II); IV-CBG, zircon from coarse biotite-granite (intrusion stage IV).

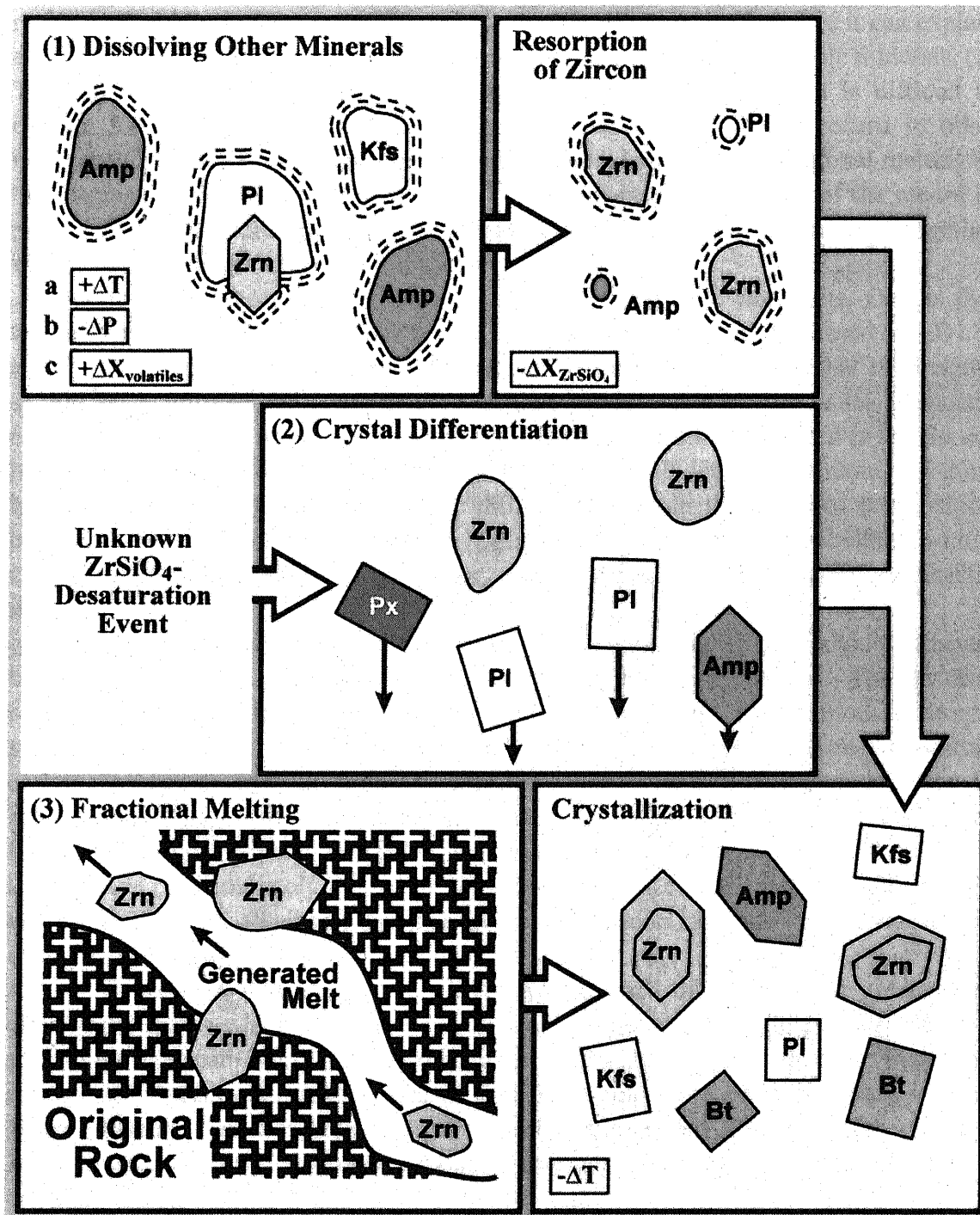


Fig. 18. Three possible explanations for forming RD on zircon surface and separation of other minerals. See text in detail.



(1) The first possibility what was the event is nearly complete melting of other minerals by any of the following three reasons; (1a) increasing temperature, (1b) decreasing pressure and (1c) addition of volatile content like fluorine. For any reason, melting of other minerals causes Zr-undersaturation of the melt; therefore it can explain easily both RD formation at zircon surface and deletion of other recordable minerals. (2) The second assumption is selective fractionation of other minerals. It is difficult to explain formation of RD but most simply explains to lack of the record in other minerals. (3) The last one is transient solidification and subsequent fractional melting of the magma system. It can very well explain to RD formation and lack of the record in present rocks by additional assumption that dissolving zircon was separated together with the generated melt from solidified rock.

In above cases, (1b) is unlikely in view of the following facts. One is that temperature decreasing would have occurred before RD formation, it is based on LD1 in core, so decompression melting would not have expected. Another is that the magma should have intruded into less shallow region because this A-type suite is mostly consisted of plutonic rock, therefore even if decompression had occurred it should not have been intense. Then, (2) is not realistic in point of high density of zircon. (1a) must be able to form RD but it seems to be difficult to explain the different composition between core and rim, for this reason if (1a) had occurred it was associated with a compositional shift of the magma system, such as inflow of high temperature basaltic magma.

All of the observed zircons which are included in II-QSy alkali feldspars contain RD (or LD1 in some cases) as nearly outermost texture. The textural relationship indicates that those alkali feldspars grew just after RD formation on zircons surface. Ridolfi et al. (2006) described that alkali feldspar crystallization had started earlier than zircon crystallization and finished roughly simultaneously with zircon in Kenyan syenite. So if the crystallization sequence can apply to II-QSy, the "old" alkali feldspar should have been presented before Zr-undersaturation event and subsequently it should have (1) completely melted or (3) left wherein as restite of fractionally melted system, then "new" alkali feldspar had grown with zircon after the Zr-undersaturation event of any of (1a), (1c) or (3).

In contrast, IV-CBG zircon grains have LD2 and thick outermost igneous rim even in the grains which have included in alkali feldspar and plagioclase. It indicates that those feldspars must have grown after enclosing melt in zircons. Based on microscopic observation plagioclases of IV-CBG would have crystallized earlier than alkali feldspars, however both feldspars should have started the crystallization after Zr-undersaturation event even when the Kenyan crystallization sequence can be applied on IV-CBG magma or not.

Consequently, the magmatic event which formed RD formed and deleted the record in the other minerals except zircon would be (1a) inflow of high temperature magma which is associated with a compositional shift, (1c) addition of volatile fluid probably rich in fluorine and (3) transient solidification and subsequent fractional melting. Considering the partial development of RD and early crystallization of alkali

feldspar in peralkalic melt, it would be suggested that (3) is the most likely to be possible; however above interpretation is still speculative at present, so it is necessary to have evidences for revealing the magmatic event and magmatic evolution of this A-type suite.

#### 5.4 Melt compositions around Zr-undersaturation event

As mentioned above, the chemical composition of zircon core and rim are clearly different in both rock samples. In comparison with II-QSy zircons, IV-CBG zircons have higher Hf concentration, lower U concentration and more mildly-sloped distribution on the U-Y diagram (Fig. 17).

Rubatto and Hermann (2007) and Luo and Ayers (2009) carried out experimental studies about zircon/melt partition coefficients including  $D_U$  and  $D_Y$ . Their  $D_{\text{zircon/melt}}^{\text{U and Y}}$  shown in Fig. 19 are summarized as follows; (1)  $D_U$  and  $D_Y$  keep roughly parallel relationship through temperature change, (2)  $D_U$  highly increases than  $D_Y$  as the melt alkalinity increases and (3) in shallow setting  $D_U$  increases close to  $D_Y$  as the pressure decreases. The inversion of  $D_U$  and  $D_Y$  was reported only on (2), so most likely change between two magmas would be alkalinity decreasing. However such compositional change should be accompanied by changes of U and/or Y concentration of the melt. Furthermore, these studies are based on hydrous melt, hence the estimation of melt composition of which forms each cores and rims of II-QSy and IV-CBG is very difficult.

#### 5.5 Discrete development of two magmas

As pointed out above, the chemical compositions of core and rim are different in zircons from each rock sample. On the other hand, compositional differences have also been confirmed among cores and among rims of zircons from II-QSy and IV-CBG, likewise between II-QSy zircon rims and IV-CBG zircon cores. This indicates that all pairs of cores and rims in those zircons would not have been crystallized from same magma. However, both zircons of II-QSy and IV-CBG commonly share same internal textures such as LD1, RD, LD2 and remained core, therefore different composition at early-stage and subsequent same (or similar) developing processes might have existed on those magmas evolution.

Murakami et al. (1989) estimated the origin of Cape Ashizuri Ring Complex to be similar to Loiselle and Wones (1979). In consideration of the zircon internal texture observed in this study, magmatic differentiation of the lithofacies which we can find at present would not have occurred at shallow crust after intrusion along extensional crack. It might have occurred at lower crust, or perhaps the magmas had been generated

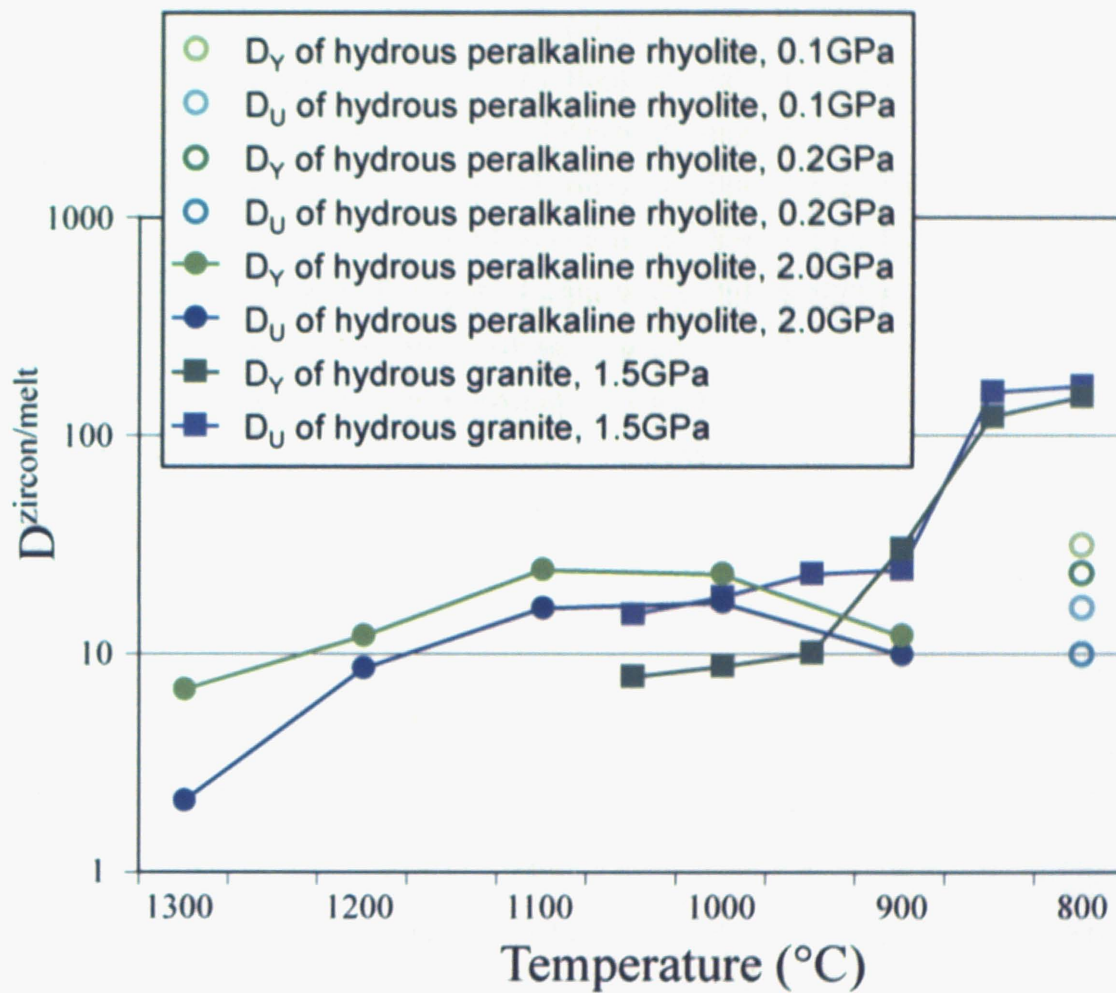


**Fig. 19.** Reviewing diagram of  $D^{\text{zircon/melt}}$  on Y and U for each zircon-equilibrated temperature. Datas are extracted from Luo and Ayers (2009) for hydrous peralkaline rhyolite melt and Rubatto and Hermann (2007) for hydrous granitic melt.  $\text{SiO}_2$  content of each starting material is approximately 70 wt% for hydrous peralkaline rhyolite and 60 wt% for hydrous granite.

individually. This “different generation and similar evolution” may be the key to reveal petrogenesis of uncommon occurrence of A-type granite such as Cape Ashizuri Ring Complex.

## **Conclusions of Chapter 2**

- (1) Various internal textures were newly found in zircon from Cape Ashizuri Ring Complex.
- (2) Textural and chemical features of the internal textures were described.
- (3) Based on the feature, the secondary internal textures were classified into three types; RD, LD and HD.
- (4) The formation mechanisms of three secondary internal textures were estimated.
- (5) Six growth stages of the zircon were suggested from their textural relationship.
- (6) Non-fractional chemical change of early magma of the ring complex and the three possible events were suggested by textural and chemical features of zircon.
- (7) Depending on chemical difference and textural similarity of the zircons, different generation and similar magmatic development were strongly suggested for two lithofacies of Cape Ashizuri Ring Complex.

## **Conclusions**

- (1) Two unique accessory minerals were found from Cape Ashizuri Ring Complex and examine in detail; thorite and zircon.
- (2) Crystallographical, micro-textural and chemical descriptions were carried out on the two accessory minerals.
- (3) Based on experimental data and detailed observation, formation mechanism of the internal nanostructure and microtextures of the minerals were discussed.
- (4) The possibilities that these mineralogical features of the two accessory minerals contribute to solve geochronological and petrological problems were suggested.

## **Acknowledgments**

I gratefully acknowledge for helpful advices and technical supports of Prof. S. Miyashita and Dr. Y. Adachi at Niigata University. Prof. N. Tsuchiya at Iwate University and Dr. M. Hoshino at AIST are also acknowledged for technical support on EPMA analysis. The collecting of rock samples in Cape Ashizuri area was kindly supported by D. Watanabe at Ministry of the Environment. I thank Prof. J. Akai and all my colleagues for their meaningful comments.

## References

- Best, M. G. & Christiansen, E. H. (2001): Igneous petrology. *Blackwell Science*, 458p.
- Bomparola, R. M., Ghezzo, C., Belousova, E., Griffin, W. L. & O'Reilly, S. Y. (2007): Resetting of the U-Pb Zircon System in Cambro-Ordovician Intrusives of the Deep Freeze Range, Northern Victoria Land, Antarctica. *Jour. Petr.* **48**, 327-364.
- Bonin, B. (1982): Les granites des complexes annulaires. *BRGM*, 183p.
- Bonin, B. (2007): A-type granites and related rocks: Evolution of a concept, problems and prospects. *Lithos* **97**, 1-29.
- Bowden, P. & Kinnaird, J. A. (1984): The petrology and geochemistry of alkaline granites from Nigeria. *Phys. Earth. Planet. In.*, **35**, 199-211.
- Brooks, C. K. (1969): On the distribution of zirconium and hafnium in the Skaergaard intrusion, East Greenland. *Geochim. Cosmochim. Acta*, **33**, 357-374.
- Carrez, P., Forterre, C., Braga, D. & Leroux H. (2003): Phase separation in metamict zircon under electron irradiation. *Nucl. Instrum. Meth. Phys. Res.* **B211**, 549-555.
- Cawley, J. M. (1992): Electron diffraction techniques. *Oxford University Press*, 423p.
- Claiborne, L. L., Miller, C. F. & Wooden, J. L. (2010): Trace element composition of igneous zircon: a thermal and compositional record of the accumulation and evolution of a large silicic batholith, Spirit Mountain, Nevada. *Contrib. Mineral. Petrol* **160**, 511-531.
- Clemens, J. D., Holloway, J. R. & White, A. J. R. (1986): Origin of an A-type granite: Experimental constraints. *Am. Mineral.* **71**, 317-324.
- Collins, W. J., Beams, S. D., White, A. J. R. & Chappell, B. W. (1982): Nature and Origin of A-type Granites with Particular Reference to Southeastern Australia. *Contrib. Mineral. Petrol.* **80**, 189-200.
- Corfu, F., Hanchar, J. M., Hoskin, P. W. O. & Kinny, P. (2003): Atlas of Zircon Textures. *Rev. Mineral. Geochem.* **53**, 469-500.
- Currie, K. L. & van Breemen, O. (1996): The origin of rare minerals in the Kipawa syenite complex, western Quebec. *Can. Mineral.* **34**, 435-451.
- da Silva, L. C., McNaughton, N. J. & Fletcher, I. R. (2005): SHRIMP U-Pb zircon

- geochronology of Neoproterozoic crustal granitoids (Southern Brazil): A case for discrimination of emplacement and inherited ages. *Lithos* **82**, 503-525.
- Ewing, R. C. (2001): The design and evaluation of nuclear-waste forms: clues from mineralogy. *Can. Mineral.* **39**, 697-715.
- Farges, F. & Calas, G. (1991): Structural analysis of radiation damage in zircon and thorite: An X-ray absorption spectroscopic study. *Am. Mineral.* **76**, 60-73.
- Feltz, A. (1993): Amorphous inorganic materials and glasses. *Weinheim*, 446p.
- Finch, R. J. & Hanchar, J. M. (2003): Structure and chemistry of zircon and zircon-group minerals. *Rev. Mineral. Geochem.* **53**, 1-25.
- Förster, H. J. (2006): Composition and origin of intermediate solid solutions in the system thorite-xenotime-zircon-coffinite. *Lithos* **88**, 35-55.
- Fu, B., Zeb Page, F., Cavosie, A. J., Fournelle, J., Kita, N. T., Lackey, J. S., Wilde, S. A. & Valley, J. W. (2008): Ti-in-zircon thermometry: applications and limitations. *Contrib. Mineral. Petrol* **156**, 197-215.
- Grant, M. L., Wilde, S. A., Wu, F. & Yang, J. (2009): The application of zircon cathodoluminescence imaging, Th-U-Pb chemistry and U-Pb ages in interpreting discrete magmatic and high-grade metamorphic events. *Chem. Geol.* **261**, 155-171.
- Harris, L. A. (1959): Preliminary study of the phase equilibria diagram of ThO<sub>2</sub>-SiO<sub>2</sub>. *J. Am. Ceram. Soc.* **42**, 74-77.
- Hayashi, S., Ishihara, S. & Sakamaki Y. (1969): Uranium in the decomposed granitic rocks at Cape Ashizuri, Kochi Prefecture, with special reference to the green uranothorite. *Reports, Geological Survey of Japan* **232**, 93-105 (in Japanese with English abstr.).
- Hiess, J., Nutman, A. P., Bennett, V. C. & Holden, P. (2008): Ti-in-zircon thermometry applied to contrasting Archean metamorphic and igneous systems. *Chem. Geol.* **247**, 323-338.
- Holland, H. D. & Gottfried, D. (1955): The effect of nuclear radiation on the structure of zircon. *Acta Crystallogr.* **8**, 291-300.
- Hoshino, M. & Ishihara, S. (2007): REE-bearing minerals of the Late Cretaceous ilmenite-series granites of the Inner Zone of Southwest Japan. *Resource Geol.* **57**,



103-114.

- Hoskin, P. W. O. (2000): Patterns of chaos: fractal statistics and the oscillatory chemistry of zircon. *Geochim. Cosmochim. Acta* **64**, 1905-1923.
- Hoskin, P. W. O. (2005): Trace-element composition of hydrothermal zircon and the alteration of Hadean zircon from the Jack Hills, Australia. *Geochim. Cosmochim. Acta* **69**, 637-648.
- Hoskin, P. W. O. & Black, L. P. (2000): Metamorphic zircon formation by solid-state recrystallization of protolith igneous zircon. *J. Metamorph. Geol.* **18**, 423-439.
- Hoskin, P. W. O. & Schaltegger, U. (2003): The Composition of Zircon and Igneous and Metamorphic Petrogenesis. *Rev. Mineral. Geochem.* **53**, 27-62.
- Iizumi, S. & Murakami, N. (1985): Sr isotope ratio in Cape Ashizuri Igneous Complex. *The 92th Annual Meeting of the Geological Society of Japan*, 338.
- Imaoka, T., Nakashima, K. & Murakami, N. (1991): Gallium in A-type granites from Cape Ashizuri, Kohchi Prefecture, Southwest Japan. *J. Mineral. Petrol. Econ. Geol.* **86**, 354-363 (in Japanese with English Abstr.).
- Janeczek, J. & Ewing, R. (1996): Phosphatian coffinite with rare earth elements and Ce-rich françoisite-(Nd) from sandstone beneath a natural fission reactor at Bangombé, Gabon. *Mineral. Mag.* **60**, 665-669.
- Kebede, T., Horie, K., Hidaka, H. & Terada, K. (2007): Zircon 'microvein' in peralkaline granitic gneiss, western Ethiopia: Origin, SHRIMP U-Pb geochronology and trace element investigations. *Chem. Geol.* **242**, 76-102.
- Koreshkova, M. Y., Downes, H., Nikitina, L. P., Vladykin, N. V., Larionov, A. N. & Sergeev, S. A. (2009): Trace element and age characteristics of zircons in granulite xenoliths from the Udachnaya kimberlite pipe, Siberia. *Precambrian Res.* **168**, 197-212.
- Lee, J. K. W. & Tromp, J. (1995): Self-induced fracture generation in zircon. *J. Geophys. Res.* **100**, 17753-17770.
- Lian, J., Zhang, J. M., Pointeau, V., Zhang, F. X., Lang, M., Lu, F. Y., Poinssot, C. & Ewing, R. C. (2009): Response of synthetic coffinite to energetic ion beam irradiation. *J. Nucl. Mater.* **393**, 481-486.
- Linnen, R. L. & Keppler, H. (2002): Melt composition control of Zr/Hf fractionation in

- magmatic processes. *Geochim. Cosmochim. Acta* **66**, 3293-3301.
- Loiselle, M. C. & Wones, D. R. (1979): Characteristics and origin of anorogenic granites. *Abstr. Programs Geol. Soc. Am.* **11**, 468.
- Luo, Y. & Ayers, J. C. (2009): Experimental measurements of zircon/melt trace-element partition coefficients. *Geochim. Cosmochim. Acta* **73**, 3656-3679.
- Martin, R. F. (2006): A-type granites of crustal origin ultimately result from open-system fenitization-type reactions in an extensional environment. *Lithos* **91**, 125-136.
- Meldrum, A., Boatner, L. A., Zinkle, S. J., Wang, Shi-Xin, Wang, Lu-Min & Ewing, R. C. (1999): Effects of dose rate and temperature on the crystalline-to-metamict transformation in the ABO<sub>4</sub> orthosilicates. *Can. Mineral.* **37**, 207-221.
- Meldrum, A., Zinkle, S. J., Boatner, L. A. & Ewing, R. C. (1998): A transient liquid-like phase in the displacement cascades of zircon, hafnium and thorite. *Nature* **395**, 56-58.
- Mishra, R. K., Sengupta, P., Kaushik, C. P., Tyagi, A. K., Kale, G. B. & Raj, K. (2007): Studies on immobilization of thorium in barium borosilicate glass. *J. Nucl. Mater.* **360**, 143-150.
- Murakami, N. & Imaoka, T. (1980): Petrochemistry of plutonic rocks from southwestern area of Shikoku, Japan —especially on the characteristic feature of plutonic rocks from Cape of Ashizuri—. *Geology and Paleontology of the Shimanto Belt*, 57-70 (in Japanese with English abstr.).
- Murakami, N. & Imaoka, T. (1985): Rapakivi granites from Cape of Ashizuri, Kochi Prefecture, Southwest Japan. *Jour. Geol. Soc. Japan* **91**, 179-194.
- Murakami, N., Imaoka, T. & Uozumi, S. (1989): Ring Complex of Cape of Ashizuri, and its mode of emplacement, Kochi Prefecture, Southwest Japan. *Monograph-Association for the Geological Collaboration in Japan*, **36**, 115-142 (in Japanese with English abstr.).
- Murakami, N., Kanisawa, S. & Ishikawa, K. (1983): High fluorine content of Tertiary igneous rocks from Cape of Ashizuri, Kochi Prefecture, Southwest Japan. *J. Japan. Assoc. Mineral. Petrol. Econ. Geol.* **78**, 497-504 (in Japanese with English abstr.).
- Murakami, N. & Masuda, Y. (1984): Trace elements in the Tertiary igneous rocks from Cape of Ashizuri, Kōchi Prefecture, Southwest Japan. *J. Japan. Assoc. Mineral.*

*Petrol. Econ. Geol.* **79**, 318-328 (in Japanese with English abstr.).

Murakami, T., Chakoumakos, B. C., Ewing, R. C., Lumpkin, G. R. & Weber, W. J. (1991): Alpha-decay event damage in zircon. *Am. Mineral.* **76**, 1510-1532.

Nasdala, L., Irmer, G. & Jonckheere, R. (2002): Radiation damage ages: Practical concept or impractical vision? – Reply to two comments on "Metamictisation of natural zircon: Accumulation versus thermal annealing of radioactivity-induced damage", and further discussion. *Contrib. Mineral. Petrol.* **143**, 758-765.

Nemchin, A. A., Giannini, L. M., Bodorkos, S. & Oliver, N. H. S. (2001): Ostwald ripening as a possible mechanism for zircon overgrowth formation during anatexis: Theoretical constraints, a numerical model, and its application to pelitic migmatites of the Tickalara Metamorphics, northwestern Australia. *Geochim. Cosmochim. Acta* **65**, 2771-2787.

Nemchin, A. A. & Pidgeon, R. T. (1997): Evolution of the Darling Range Batholith, Yilgarn Craton, Western Australia: a SHRIMP zircon study. *J. Petrol.* **38**, 625-649.

Nutman, A. P., McGregor, V. R., Shiraishi, K., Friend, C. R. L., Bennett, V. C. & Kinny, P. D. (2002): >3850 Ma BIF and mafic inclusions in the early Archaean Itsaq Gneiss Complex around Akilia, southern West Greenland? The difficulties of precise dating of zircon-free protoliths in migmatites. *Precambrian Res.* **117**, 185-224.

Orejana, D., Villaseca, C., Armstrong, R. A. & Jeffries, T. E. (in press): Geochronology and trace element chemistry of zircon and garnet from granulite xenoliths: Constraints on the tectonothermal evolution of the lower crust under central Spain. *Lithos*, in press.

Pabst, A. (1952): The metamict state. *Am. Mineral.* **37**, 137-157.

Palenik, C. S., Nasdala, L. & Ewing, R. C. (2003): Radiation damage in zircon. *Am. Mineral.* **88**, 770-781.

Pelleter, E., Cheilletz, A., Gasquet, D., Mouttaqi, A., Annich, M., El Hakour, A., Deloule, E. & Feraud, G. (2007): Hydrothermal zircons: A tool for ion microprobe U-Pb dating of gold mineralization (Tamlalt-Menhouhou gold deposit-Morocco). *Chem. Geol.* **245**, 135-161.

Redfern, S. A. T. (1996): Length scale dependence of high-pressure amorphization: the static amorphization of anorthite. *Mineral. Mag.* **60**, 493-498.

- Ridolfi, F., Renzulli, A., Macdonald, R. & Upton, B. G. J. (2006): Peralkaline syenite autoliths from Kilombe volcano, Kenya Rift Valley: Evidence for subvolcanic interaction with carbonatitic fluids. *Lithos* **91**, 373-392.
- Rubatto, D. (2002): Zircon trace element geochemistry: partitioning with garnet and the link between U-Pb ages and metamorphism. *Chem. Geol.* **184**, 123-138.
- Rubatto, D. & Hermann, J. (2007): Experimental zircon/melt and zircon/garnet trace element partitioning and implications for the geochronology of crustal rocks. *Chem. Geol.* **241**, 38-61.
- Salje, E. K. H., Chrosch, J. & Ewing, R. C. (1999): Is "metamictization" of zircon a phase transition?. *Am. Mineral.* **84**, 1107-1116.
- Seydoux-Guillaume, A. M., Montel, J. M., Wirth, R. & Moine, B. (2009): Radiation damage in diopside and calcite crystals from uranothorianite inclusions. *Chem. Geol.* **261**, 318-332.
- Shibata, K. & Nozawa, T. (1968): K-Ar ages of granitic rocks of Ashizuri-Misaki, Takatsukiyama and Omogo, Shikoku, Japan. *Bull. Geol. Surv. Japan* **19**, 223-228.
- Taylor, F. W., Isacks, B. L., Jouannic, C., Bloom, A. L. & Dubois, J. (1980): Coseismic and Quaternary vertical tectonic movements, Santo and Malekula islands, New Hebrides island arc. *J. Geophys. Res.* **85**, 5367-5381.
- Tomaschek, F., Kennedy, A. K., Villa, I. M., Lagos, M. & Ballhaus, C. (2003): Zircons from Syros, Cyclades, Greece-Recrystallization and Mobilization of Zircon During High-Pressure Metamorphism. *J. Petrol.* **44**, 1977-2002.
- van Breemen, O. & Currie, K. L. (2004): Geology and U-Pb geochronology of the Kipawa Syenite Complex - a thrust related alkaline pluton - and adjacent rocks in the Grenville Province of western Quebec. *Can. J. Earth Sci.* **41**, 431-455.
- Vance, E. R. & Anderson, B. W. (1972): Study of metamict Ceylon zircons. *Mineral. Mag.* **38**, 605-613.
- Vavra, G., Gebauer, D., Schmid, R. & Compston, W. (1996): Multiple zircon growth and recrystallization during polyphase Late Carboniferous to Triassic metamorphism in granulites of the Ivrea Zone (Southern Alps): an ion microprobe (SHRIMP) study. *Contrib. Mineral. Petrol.* **122**, 337-358.
- Vavra, G. & Hansen, B. T. (1991): Cathodoluminescence studies and U/Pb dating of zircons in pre-Mesozoic gneisses of the Tauern Window: Implications for the

Penninic basement evolution. *Geol. Rundsch. Z. Allg. Geol.* **80**, 703-715.

Watson, E. B. & Liang, Y. (1995): A simple model for sector zoning in slowly grown crystals: Implications for growth rate and lattice diffusion, with emphasis on accessory minerals in crustal rocks. *Am. Mineral.* **80**, 1179-1187.

Williams, I. S. & Claesson, S. (1987): Isotopic evidence for the Precambrian provenance and Caledonian metamorphism of high grade paragneisses from the Seve Nappes, Scandinavian Caledonides II. Ion microprobe zircon U-Th-Pb. *Contrib. Mineral. Petrol.* **97**, 205-217.

Wu, Y. -B., Zheng, Y. -F., Zhao, Z. -F., Gong, B., Liu, X. M., & Wu, F. -Y. (2006): U-Pb, Hf and O isotope evidence for two episodes of fluid- assisted zircon growth in marble-hosted eclogites from the Dabie orogen. *Geochim. Cosmochim. Acta* **70**, 3743-3761.